

Evolution of perturbations and cosmological constraints in decaying dark matter models with arbitrary decay mass products

Shohei Aoyama,¹ Toyokazu Sekiguchi,^{1,2} Kiyotomo Ichiki³ and Naoshi Sugiyama^{1,3,4}

¹Department of Physics and Astrophysics, Nagoya University, Nagoya 464-8602, Japan

²University of Helsinki and Helsinki Institute of Physics, P.O. Box 64, FI-00014, Helsinki, Finland

³Kobayashi-Maskawa Institute for the Origin of Particles and the Universe, Nagoya University, Nagoya 464-8602, Japan

⁴Kavli Institute for the Physics and Mathematics of the Universe (Kavli IPMU), The University of Tokyo, Chiba 277-8582, Japan

Abstract. Decaying dark matter (DDM) is a candidate which can solve the discrepancies between predictions of the concordance Λ CDM model and observations at small scales such as the number counts of companion galaxies of the Milky Way and the density profile at the center of galaxies. Previous studies are limited to the cases where the decay particles are massless and/or have almost degenerate masses with that of mother particles. Here we expand the DDM models so that one can consider the DDM with arbitrary lifetime and the decay products with arbitrary masses. We calculate the time evolutions of perturbed phase-space distribution functions of decay products for the first time and study effects of DDM on the temperature anisotropy in the cosmic microwave background and the matter power spectrum at present. From a recent observational estimate of σ_8 , we derive constraints on the lifetime of DDM and the mass ratio between the decay products and DDM. We also discuss implications of the DDM model for the discrepancy in the measurements of σ_8 recently claimed by the Planck satellite collaboration.

Keywords: dark matter, cosmological perturbation theory, large scale structure

Contents

1	Introduction	1
2	Model of DDM and Boltzmann equation	3
2.1	DDM model and set up	3
2.2	Boltzmann equations	4
2.2.1	Mother particles	6
2.2.2	Daughter particles	7
3	Time evolutions of perturbations	9
3.1	A case of non-relativistic decay	9
3.1.1	Perturbations crossing the horizon after the decay time	10
3.1.2	Perturbations crossing the horizon before the decay time	11
3.2	A case of relativistic decay	13
3.2.1	Perturbations crossing the horizon after the decay time	13
3.2.2	Perturbations crossing the horizon before the decay time	14
4	Signatures in cosmological observables	16
4.1	Effects on C_l	16
4.2	Effects on $P(k)$	19
5	Discussion	20
5.1	Implication on the anomaly in estimated σ_8 from Planck	23
6	Conclusion	25
A	Initial condition for the perturbed distribution functions of the daughter particles	27
A.1	Radiation-dominated era	28
A.2	Matter-dominated era	29

1 Introduction

Numerous kinds of astrophysical observations suggest the existence of dark matter, which has no electro-magnetic or strong interactions with other particles in the Universe. It is necessary for explaining the observed phenomena such as flat rotation curves of galaxies, anisotropies in the cosmic microwave background (CMB) and the formation of large scale structure within the age of the Universe, $t_{\text{age}} = 13.8$ Gyr [1]. In particular, to explain the hierarchical formation of the cosmic structure, dark matter should have very small momentum hence so-called cold dark matter (CDM) becomes the standard model of dark matter.

However, while it is widely believed that dark matter consists of particles beyond the Standard Model, we have little knowledge on the nature of dark matter. Thus, for

example, it remains possible that dark matter decays into other particles with smaller masses. This kind of dark matter is called decaying dark matter (DDM). By constraining the lifetime of DDM, we can obtain the nature of dark matter and information about a particle theory lying behind it. While the CDM model is widely consistent with observations on cosmological scales, there exist some discrepancies at sub-galactic scales between the model predictions by N-body simulations and astronomical observations. Well known examples are the "cusp problem" [2, 3], i.e., the over-concentration problem of the inner core of galaxies, and the "missing satellite problem" [4] or the "too big to fail problem" [5], where the number or properties of satellite galaxies of the Milky Way do not match the results from numerical simulations. DDM is often discussed as a remedy to such small-scale CDM problems, for example, see Cen [6]. The DDM model, however, should pass the tests from precise cosmological observations, such as measurements of the CMB and the large scale structure of the universe. One of the aims of this paper is therefore to give a complete set of perturbation equations of the DDM model with decay products having arbitrary masses, and show some evolutions of density perturbations in the DDM model to compare them with recent cosmological observations.

Cosmological implications of DDM have been studied by several authors [6–21]. Among them, Kaplinghat [10] and Huo [19] have considered models in which dark matter decays into two "daughter" particles¹ well before the matter-radiation equality epoch. They calculated time evolution of perturbations and set constraints on the mass ratio and the life time of DDM from the free streaming scale of daughter particles. The former considered the DDM which decays into a massive particle and massless one in the early Universe. They computed the matter power spectrum and discussed the effects of free-streaming of the decay products by considering the phase-space density of the massive daughter particle. The latter computed the CMB power spectrum in addition to the matter power spectrum. Moreover, DDM models in which the mass difference between the mother and the massive daughter particles Δm is much smaller than the mass of the mother particles are studied in refs. [17, 18, 21, 22]. In particular, Peter [17] has considered effects of the recoil energy of the daughter particles on the halo mass-concentration and galaxy-cluster mass function using N-body simulations and set constraints on the lifetime of DDM and Δm in terms of the kick velocity v_{kick} by demanding that the daughter particles in halos with mass $M = 10^{12} M_{\odot}$ do not escape from the halos and destroy the gravitational potential. She also set constraints by using weak lensing measurements and X-ray observations. Wang et al. have analyzed N-body simulations with DDM and focused on the statistical properties of the transmitted Lyman- α (Ly- α) forest flux. By comparing the data of the Sloan Digital Sky Survey (SDSS) and WMAP 7 with their simulation data, they set a constraint on the life time of DDM as $\Gamma^{-1} > 40$ Gyr where $v_{\text{kick}} \gtrsim 50$ km/s [22]. However, previous studies so far could not deal with DDM models where mother particles decay into particles with arbitrary mass at late times (i.e. after the matter-radiation equality). This is what we will explore in this paper.

In this paper, we investigate models of DDM which decays into two daughter

¹We call progenitor particle "mother" particle.

particles. We study linear cosmological perturbations in the DDM model without approximations such that the decay products are massless or highly non-relativistic. Instead, we directly solve the Boltzmann equations for the mother and daughter particles and follow the time evolutions of their distribution functions in the discretized phase space. In this formulation, one can set masses of both daughter particles to arbitrary values. While our formulation and numerical implementation can deal with arbitrary lifetime and/or masses of daughter particles, to minimize complication, we assume that DDM decays after cosmological recombination into two particles one of which has a finite mass and the other is massless.

Here, we basically follow the notation of Ma and Bertschinger [23]. We adopt natural units with $c = \hbar = k_B = 1$. The proper and conformal time are denoted by t and τ , respectively. A dot represents partial derivative with respect to the conformal time, i.e., $\dot{f} \equiv \partial f / \partial \tau$. A quantity with a subscript "*" indicates its value at cosmological recombination.

The layout of this paper is as follows. In the following section, we introduce our DDM model and present the Boltzmann equations, which describe the perturbation evolutions. In addition, we also describe how we solve the equations numerically. Section 3 denotes time evolutions of perturbations in the DDM model. Effects on cosmological observables including the angular power spectrum of the CMB anisotropy C_l and the matter power spectrum $P(k)$ are discussed in section 4. In section 5, we discuss some interpretations for the effects of the decay of dark matter and derive a constraint on the DDM model from an observed value of σ_8 . Finally, section 6 concludes this paper.

2 Model of DDM and Boltzmann equation

2.1 DDM model and set up

In this work, we consider a model of DDM (M) which decays into two particles (D1, D2) well after cosmological recombination,

$$M \rightarrow D1 + D2 \quad (\text{with } \Gamma^{-1} \gg t_*), \quad (2.1)$$

where Γ is the decay rate of DDM.

Throughout this paper, we assume a variant of the concordance flat power-law Λ CDM model where CDM is replaced with DDM, and consider cosmological perturbations. The model is specified with the following cosmological parameters:

$$(\Omega_b, \Omega_{M\emptyset}, h_\emptyset, \tau_{\text{reion}}, n_s, A_s, \Gamma, m_{D1}/m_M, m_{D2}/m_M), \quad (2.2)$$

where Ω_b and $\Omega_{M\emptyset}$ are the density parameters of baryons and mother particles, respectively, h_\emptyset is the reduced Hubble constant estimated assuming that the DDM does not decay, τ_{reion} is the optical depth of reionization, and n_s and A_s are respectively the spectral index and amplitude of the primordial curvature perturbation at $k = 0.002 \text{ Mpc}^{-1}$. Here and in the following, the subscript \emptyset indicates quantities

which are estimated assuming $\Gamma = 0$. Following the WMAP 7-year results [24]², we fix $(\Omega_b, \Omega_{M0}, h_0, \tau_{\text{reion}}, n_s, A_s)$ to $(0.0454, 0.226, 0.704, 0.088, 0.967, 2.43 \times 10^{-9})$. With the parameterization eq. (2.2), the genuine Hubble constant h and the density parameter of mother particles Ω_M are derived parameters which can be obtained by solving the background evolution. It should be noted that these values of parameters are not necessary to be the best fitting values to WMAP-7 year data in the DDM model. These values are adopted only for a reference. Regarding m_{D2}/m_M , while the formalism we present in this section is applicable for arbitrary masses of the daughter particles, as is stated in introduction, we in the rest of this paper assume that the mass of one of the daughter particles can be nonzero and the other one is massless. Thus, Γ and m_{D1}/m_M are treated as free parameters with m_{D2}/m_M being fixed to zero. Subscripts "M", "D1" and "D2" indicate the mother, massive daughter, and massless daughter particles, respectively.

2.2 Boltzmann equations

In this paper, we choose the synchronous gauge of the mother particles to describe cosmological linear perturbations. The line element is given by

$$ds^2 = a(\tau)^2 \{ d\tau^2 + (\delta_{ij} + h_{ij}(\mathbf{x}, \tau)) dx^i dx^j \} , \quad (2.3)$$

where a is the scale factor and h_{ij} represents the metric perturbations. In terms of Fourier components, h_{ij} can be given as

$$h_{ij}(\mathbf{x}, \tau) = \int d^3k \left(h_L(\mathbf{k}, \tau) \hat{k}_i \hat{k}_j + 6\eta_T(\mathbf{k}, \tau) (\hat{k}_i \hat{k}_j - \frac{1}{3} \delta_{ij}) \right) \exp(i\mathbf{k} \cdot \mathbf{x}) , \quad (2.4)$$

where $\mathbf{k} \equiv k\hat{\mathbf{k}}$ is a wave number vector and $\hat{\mathbf{k}}$ is the unit vector of \mathbf{k} . In the rest of this section, we focus on a single mode of perturbations with \mathbf{k} and often abbreviate dependences of perturbed variables on \mathbf{k} .

The Boltzmann equation which describes time evolution of a phase-space distribution function $f(\mathbf{x}, \mathbf{q}, \tau)$ can be written as

$$\frac{\partial f}{\partial \tau} + \frac{dx^i}{d\tau} \frac{\partial f}{\partial x^i} + \frac{dq}{d\tau} \frac{\partial f}{\partial q} + \frac{dn^i}{d\tau} \frac{\partial f}{\partial n^i} = \left(\frac{\partial f}{\partial \tau} \right)_C , \quad (2.5)$$

where \mathbf{q} is the comoving momentum, which is related to the physical momentum \mathbf{p} by $\mathbf{q} = a\mathbf{p}$, and q and $n^i = q^i/q$ are respectively the norm and the direction of \mathbf{q} . For a perturbation mode with \mathbf{k} , the second term of the left hand side can be rewritten as $i(\hat{\mathbf{k}} \cdot \mathbf{n})(q/\varepsilon)f$, where ε is the comoving energy. In the left hand side, the third term can be rewritten in terms of the metric perturbations by adopting the geodesic equation

$$p^0 \frac{dp^\mu}{d\tau} + \Gamma^\mu_{\alpha\beta} p^\alpha p^\beta = 0 . \quad (2.6)$$

² Recently, the cosmological parameters derived by Planck have been reported [25]. Since the estimated values of $\Omega_b h^2$ and $\Omega_c h^2$ change from those of the WMAP 7-year results only by several percent, results and constraints presented in this paper may not be affected significantly when the cosmological parameters from Planck are adopted.

In particular, time-component ($\mu = 0$) of eq. (2.6) gives $dq/d\tau$ as

$$\frac{dq}{d\tau} = \dot{\eta}_T - \frac{1}{2} \left(\dot{h}_L + 6\dot{\eta}_T \right) (\hat{\mathbf{k}} \cdot \mathbf{n})^2 . \quad (2.7)$$

The fourth term of the left hand side of eq. (2.5) can be neglected to the first order, because both $(dn^i/d\tau)$ and $(\partial f/\partial n^i)$ are first-order quantities in the flat Universe.

The right hand side of eq. (2.5) is the collision term, which also describes effects of decay or creation of particles on the distribution function. Aoyama et al. [26] provided those for the mother and daughter particles. In this paper, we assume that momenta of the mother particles are negligibly small compared with the mass. Under this assumption in conjunction with our choice of gauge, the distribution function of the mother particles should be proportional to the delta function of \mathbf{q} . Then we obtain

$$f_M(q, \mathbf{n}, \tau) = N_M(\tau) \delta^{(3)}(\mathbf{q}) , \quad (2.8)$$

where N_M is the *comoving* number density of the mother particles. Then the collision terms can be recast into [26]

$$\mathbf{M} : \left(\frac{\partial f_M}{\partial \tau} \right)_C = -a\Gamma f_M , \quad (2.9)$$

$$\mathbf{D}m : \left(\frac{\partial f_{Dm}}{\partial \tau} \right)_C = \frac{a\Gamma N_M}{4\pi q^2} \delta(q - ap_{D\max}) , \quad (2.10)$$

where $p_{D\max}$ is the initial physical momentum of decay particles in the rest frame of the mother particles, which is given by

$$p_{D\max} = \frac{1}{2} \left[m_M^2 - 2(m_{D1}^2 + m_{D2}^2) + \frac{(m_{D1}^2 + m_{D2}^2)^2}{m_M^2} \right]^{1/2} . \quad (2.11)$$

Note that collision terms are the same for both the daughter particles. For later convenience, we introduce τ_q which is the conformal time when the daughter particles with a comoving momentum q are produced, i.e.,

$$q = a(\tau_q) p_{D\max} . \quad (2.12)$$

From eqs. (2.7), (2.9) and (2.10), the Boltzmann equations for the mother and the daughter particles can be written as

$$\mathbf{M} : \frac{\partial f_M}{\partial \tau} + i \frac{qk}{\varepsilon_M} (\hat{\mathbf{k}} \cdot \mathbf{n}) f_M + q \frac{\partial f_M}{\partial q} \left[\dot{\eta}_T - \frac{1}{2} (\dot{h}_L + 6\dot{\eta}_T) (\hat{\mathbf{k}} \cdot \mathbf{n})^2 \right] = -a\Gamma f_M \quad (2.13)$$

$$\begin{aligned} \mathbf{D}m : & \frac{\partial f_{Dm}}{\partial \tau} + i \frac{qk}{\varepsilon_{Dm}} (\hat{\mathbf{k}} \cdot \mathbf{n}) f_{Dm} + q \frac{\partial f_{Dm}}{\partial q} \left[\dot{\eta}_T - \frac{1}{2} (\dot{h}_L + 6\dot{\eta}_T) (\hat{\mathbf{k}} \cdot \mathbf{n})^2 \right] \\ & = \frac{a\Gamma N_M}{4\pi q^2} \delta(ap_{D\max} - q) , \end{aligned} \quad (2.14)$$

where ε_M (ε_{Dm}) is the comoving energy of the mother (m -th daughter) particles. We divide a distribution function f into the background \bar{f} and the perturbation Δf as

$$f_M(q, \mathbf{k}, \mathbf{n}, \tau) = \bar{f}_M(q, \tau) \delta^{(3)}(\mathbf{k}) + \Delta f_M(q, \mathbf{k}, \mathbf{n}, \tau) , \quad (2.15)$$

$$f_{Dm}(q, \mathbf{k}, \mathbf{n}, \tau) = \bar{f}_{Dm}(q, \tau) \delta^{(3)}(\mathbf{k}) + \Delta f_{Dm}(q, \mathbf{k}, \mathbf{n}, \tau) , \quad (2.16)$$

where \bar{f} depends only on q and τ . Due to the isotropy of the background geometry, Δf can be expanded in terms of the Legendre polynomials $P_l(\hat{\mathbf{k}} \cdot \mathbf{n})$ with $l \geq 0$. Therefore we can define $\Delta f_{M(l)}$ ($\Delta f_{Dm(l)}$) as the l -th multipole moment of Δf_M (Δf_{Dm}), i.e.

$$\Delta f_M(q, \mathbf{n}, \tau) = \sum_{l=0}^{+\infty} (-i)^l (2l+1) \Delta f_{M(l)}(q, \tau) P_l(\hat{\mathbf{k}} \cdot \mathbf{n}) , \quad (2.17)$$

$$\Delta f_{Dm}(q, \mathbf{n}, \tau) = \sum_{l=0}^{+\infty} (-i)^l (2l+1) \Delta f_{Dm(l)}(q, \tau) P_l(\hat{\mathbf{k}} \cdot \mathbf{n}) . \quad (2.18)$$

2.2.1 Mother particles

By substituting eq. (2.15) into eq. (2.5), we obtain the Boltzmann equations for the mother particles as follows:

$$\text{unperturbed : } \dot{\bar{f}}_M = -a\Gamma \bar{f}_M , \quad (2.19)$$

$$\begin{aligned} \text{1st order : } & \frac{\partial \Delta f_M}{\partial \tau} + i \frac{qk}{\varepsilon_M} (\hat{\mathbf{k}} \cdot \mathbf{n}) \Delta f_M + q \frac{\partial \bar{f}_M}{\partial q} \left[\dot{\eta}_T - \frac{1}{2} (\dot{h}_L + 6\dot{\eta}_T) (\hat{\mathbf{k}} \cdot \mathbf{n})^2 \right] \\ & = -a\Gamma \Delta f_M . \end{aligned} \quad (2.20)$$

From eqs. (2.8) and (2.19), we obtain

$$\bar{f}_M(q, t) = \frac{\bar{N}_M(\tau)}{4\pi q^2} \delta(q) \quad (2.21)$$

where $\bar{N}_M(\tau) \propto \exp(-\Gamma t)$ is the mean comoving number density of the mother particles. Denoting the mean comoving number density of the mother particles without decay as $\bar{N}_{M\emptyset}$, \bar{N}_M can be given as

$$\bar{N}_M(\tau) = \bar{N}_{M\emptyset} \exp(-\Gamma t) . \quad (2.22)$$

Note that $\bar{N}_{M\emptyset}$ is constant.

According to our gauge choice, the dipole moment of the mother particles is zero. Since the mother particles do not have nonzero momentum distribution, higher-order multipole moments should vanish, i.e.,

$$\Delta f_{M(l)} = 0 \quad (\text{for } l \geq 1) . \quad (2.23)$$

On the other hand, from eqs. (2.17) and (2.20), the monopole moment $\Delta f_{M(0)}$ obeys the following equation,

$$\frac{\partial \Delta f_{M(0)}}{\partial \tau} = \frac{1}{6} \dot{h}_L q \frac{\partial \bar{f}_M}{\partial q} - a\Gamma \Delta f_{M(0)} . \quad (2.24)$$

Equations (2.19) and (2.24) can be recast into evolution equations for the mean energy density $\bar{\rho}_M$ and its perturbation $\bar{\rho}_M\delta_M$, which are defined as

$$\bar{\rho}_M \equiv \frac{1}{a^4} \int dq 4\pi q^2 \varepsilon_M \bar{f}_M, \quad (2.25)$$

$$\bar{\rho}_M \delta_M \equiv \frac{1}{a^4} \int dq 4\pi q^2 \varepsilon_M \Delta f_{M(0)}. \quad (2.26)$$

Then by integrating eqs. (2.19) and (2.24) multiplied by $4\pi q^2 \varepsilon_M / a^4$, we obtain

$$\frac{d}{d\tau} \bar{\rho}_M + 3\mathcal{H} \bar{\rho}_M = -a\Gamma \bar{\rho}_M, \quad (2.27)$$

$$\frac{d}{d\tau} [\bar{\rho}_M \delta_M] + 3\mathcal{H} \bar{\rho}_M \delta_M = -\frac{\dot{h}_L}{2} \bar{\rho}_M - a\Gamma \bar{\rho}_M \delta_M, \quad (2.28)$$

where $\mathcal{H} = \dot{a}/a$ is the conformal Hubble expansion rate. In combination, these two equations lead to

$$\dot{\delta}_M = -\frac{\dot{h}_L}{2}. \quad (2.29)$$

We note that eq. (2.29) is the same as that for CDM without decay [23]. We also note that $\bar{\rho}_M$ as $\bar{\rho}_M(\tau) = m_M \bar{N}_M(\tau) / a^3$ since the mother particles are non-relativistic.

2.2.2 Daughter particles

By substituting eq. (2.16) into eq. (2.14), one can find

$$\text{unperturbed : } \frac{\partial \bar{f}_{Dm}}{\partial \tau} = \frac{a\Gamma \bar{N}_M}{4\pi q^3 \mathcal{H}} \delta(\tau - \tau_q), \quad (2.30)$$

$$\begin{aligned} \text{1st order : } & \frac{\partial \Delta f_{Dm}}{\partial \tau} + i \frac{qk}{\varepsilon_{Dm}} (\hat{\mathbf{k}} \cdot \mathbf{n}) \Delta f_{Dm} + q \frac{\partial \bar{f}_{Dm}}{\partial q} \left[\dot{\eta}_\Gamma - \frac{1}{2} (\dot{h}_L + 6\dot{\eta}_\Gamma) (\hat{\mathbf{k}} \cdot \mathbf{n})^2 \right] \\ & = \frac{a\Gamma \bar{N}_M}{4\pi q^3 \mathcal{H}} \delta_M \delta(\tau - \tau_q). \end{aligned} \quad (2.31)$$

In deriving these equations, we used a relation

$$\delta(q - ap_{D\max}) = \frac{1}{q\mathcal{H}} \delta(\tau - \tau_q). \quad (2.32)$$

As seen from eq. (2.30) and (2.31), the unperturbed and first order perturbation equations for both the daughter particles are identical [10, 21, 26]. Therefore we can write

$$\bar{f}_{D1}(q, \tau) = \bar{f}_{D2}(q, \tau) \equiv \bar{f}_D(q, \tau). \quad (2.33)$$

As in previous works [21, 26], by solving eq. (2.30), we obtain

$$\bar{f}_D(q, \tau) = \frac{a_q \Gamma \bar{N}_M(\tau_q)}{4\pi q^3 \mathcal{H}_q} \Theta(\tau - \tau_q), \quad (2.34)$$

where $a_q = a(\tau_q)$, $\mathcal{H}_q = \mathcal{H}(\tau_q)$ and $\Theta(x)$ is the Heaviside function.

Equation (2.31) can be expanded in terms of multipole moments, which leads to a Boltzmann hierarchy for the daughter particles:

$$\frac{\partial}{\partial \tau}(\Delta f_{\text{D}m(0)}) = -\frac{qk}{\varepsilon_{\text{D}m}}\Delta f_{\text{D}m(1)} + \frac{1}{6}\dot{h}_{\text{L}}q\frac{\partial \bar{f}_{\text{D}}}{\partial q} + \frac{a\Gamma\bar{N}_{\text{M}}}{4\pi q^3\mathcal{H}}\delta_{\text{M}}\delta(\tau - \tau_q), \quad (2.35)$$

$$\frac{\partial}{\partial \tau}(\Delta f_{\text{D}m(1)}) = \frac{qk}{3\varepsilon_{\text{D}m}}(\Delta f_{\text{D}m(0)} - 2\Delta f_{\text{D}m(2)}), \quad (2.36)$$

$$\frac{\partial}{\partial \tau}(\Delta f_{\text{D}m(2)}) = \frac{qk}{5\varepsilon_{\text{D}m}}(2\Delta f_{\text{D}m(1)} - 3\Delta f_{\text{D}m(3)}) - \left(\frac{1}{15}\dot{h}_{\text{L}} + \frac{2}{5}\dot{\eta}_{\text{T}}\right)q\frac{\partial \bar{f}_{\text{D}}}{\partial q}, \quad (2.37)$$

$$\frac{\partial}{\partial \tau}(\Delta f_{\text{D}m(l)}) = \frac{qk}{(2l+1)\varepsilon_{\text{D}m}}(l\Delta f_{\text{D}m(l-1)} - (l+1)\Delta f_{\text{D}m(l+1)}) \quad (\text{for } l \geq 3) \quad (2.38)$$

By using $\Delta f_{\text{D}m(0)}$, $\Delta f_{\text{D}m(1)}$ and $\Delta f_{\text{D}m(2)}$, the perturbed energy density $\delta\rho = \bar{\rho}\delta$, perturbed pressure $\delta p = \bar{p}\pi_{\text{L}}$, energy flux θ and shear stress σ can be written as

$$\bar{\rho}_{\text{D}m}\delta_{\text{D}m} \equiv \frac{1}{a^4} \int dq 4\pi q^2 \varepsilon_{\text{D}m} \Delta f_{\text{D}m(0)}, \quad (2.39)$$

$$\bar{p}_{\text{D}m}\pi_{\text{L}m} = \frac{1}{3a^4} \int dq 4\pi q^2 \frac{q^2}{\varepsilon_{\text{D}m}} \Delta f_{\text{D}m(0)}, \quad (2.40)$$

$$(\bar{\rho}_{\text{D}m} + \bar{p}_{\text{D}m})\theta_{\text{D}m} = \frac{k}{a^4} \int dq 4\pi q^2 q \Delta f_{\text{D}m(1)}, \quad (2.41)$$

$$(\bar{\rho}_{\text{D}m} + \bar{p}_{\text{D}m})\sigma_{\text{D}m} = \frac{1}{a^4} \int dq 4\pi q^2 \frac{q^2}{\varepsilon_{\text{D}m}} \Delta f_{\text{D}m(2)}, \quad (2.42)$$

where $\bar{\rho}_{\text{D}m}$ and $\bar{p}_{\text{D}m}$ are the mean energy density and pressure of the m -th daughter particles, respectively. Here, $\pi_{\text{L}m}$, $\theta_{\text{L}m}$ and $\sigma_{\text{D}m}$ are higher-order velocity-weighted quantities since phase space integral in these are weighted by the velocity q/ε or velocity squared $(q/\varepsilon)^2$ compared with the density perturbation $\delta_{\text{D}m}$.

Equations (2.35)-(2.38) are the same as those for massive neutrinos except for the last term in eq. (2.35) (see ref. [23]), which is responsible for the creation of density perturbation of the daughter particles from that of the mother ones. While the structure of the perturbation equations may not seem to differ from that of massive neutrinos significantly, in fact their solution is far more complicated. The complication arises from the source terms (the second and third terms in the right hand side of in eq. (2.35) and the last term in eq. (2.37)). These terms contain delta functions on τ , which clearly require a specialized treatment in numerical computation.

In order to solve the perturbation equations and obtain the CMB angular power spectrum C_l as well as the matter power spectrum $P(k)$ we modified the publicly available CAMB code [27]. In particular, we need to calculate the evolution of the phase space distribution of the daughter particles $\Delta f_{\text{D}m(l)}$ at discrete values of q . In the following, we describe how we have chosen the discrete samples of q .

Roughly speaking, we need to choose the range of q where the mean number density of the daughter particles per q , $\mathcal{F}(q) \equiv q^2 \bar{f}(q, \tau_0)$, dominantly contributes to the

integrals in Eqs. (2.39)-(2.42). Let us denote the scale factor at $t = \min(t_0, \Gamma^{-1})$ as a_D . Then the location of the maximum of $\mathcal{F}(q)$ is approximately given by $q = a_D p_{D\max}$. In our analysis, we sample q in a range $10^{-4} a_D p_{D\max} \leq q \leq \min(p_{D\max}, 5a_D p_{D\max})$, with a linearly homogeneous spacing in q . Outside this range, $\mathcal{F}(q) \propto q^{1/2} \exp[-(q/a_D p_{D\max})^{3/2}]$ is less than 1/100 of the maximum value, and contributions from such a range of q would little affect the CMB and matter power spectra.³ For a range of the DDM parameters as $0.1 \leq m_{D1}/m_M \leq 1$ and $0.01 \text{ Gyr} \leq \Gamma^{-1} \leq 1000 \text{ Gyr}$, which is of our primary interest in this paper, we have found that it is sufficient to take the number of sampled q and the maximum multipole l of $\Delta f_{Dm(l)}$ to be 1000 and 45. We confirm that if we change the number of q to be 1500 and 2000 and/or the maximum l to be 60 and 100, the results we will present in Section 4 would differ by no more than 0.8%.

The initial conditions of $\Delta f_{Dm(l)}(q, \tau)$ are set as follows. When $\tau < \tau_q$, both daughter particles which have comoving momentum q have never been generated. Thus

$$\bar{f}_D(q, \tau) = \Delta f_D(q, \mathbf{n}, \tau) = 0 \quad (\text{for } \tau < \tau_q). \quad (2.43)$$

In eqs. (2.35) and (2.37), the source terms $(1/6)\dot{h}_L q (\partial \bar{f}_D / \partial q)$, $(a\Gamma \bar{N}_M / 4\pi q^3 \mathcal{H}) \delta_M \delta(\tau - \tau_q)$ and $\left((1/15)\dot{h}_L + (2/5)\dot{\eta}_T \right) q \partial \bar{f}_D / \partial q$ contain a delta function $\delta(\tau - \tau_q)$, which makes $\Delta f_{Dm(0)}$ and $\Delta f_{Dm(2)}$ arise like a step function at $\tau = \tau_q$. In order to treat these terms, we obtain the initial values by integrating eqs. (2.35) and (2.37) with τ in a infinitesimal interval around $\tau = \tau_q$. The initial values of $\Delta f_{Dm(0)}$ and $\Delta f_{Dm(2)}$ are provided in eqs. (A.5) and (A.7) in Appendix A. For $\tau > \tau_q$, $q \partial \bar{f}_D / \partial q$ becomes a smooth function of τ and the time evolutions of the perturbed distribution functions of the daughter particles can be calculated in the same way as massive neutrinos in the standard cosmology.

3 Time evolutions of perturbations

In this section, we discuss time evolutions of perturbed quantities. Hereafter we continuously assume that m_{D2} is zero, while the mass of the first daughter particles m_{D1} can vary in $[0, m_M]$. For later convenience, we respectively denote the scale factor at the decay time and the horizon crossing as a_d and a_{hc} , i.e., $t(a_d) \equiv \Gamma^{-1}$ and $\tau(a_{hc}) \equiv \pi k^{-1}$.

3.1 A case of non-relativistic decay

In this subsection, we consider a case with $m_{D1} \simeq m_M$, which we refer to as non-relativistic decay. As a representative value, we here adopt $m_{D1} = 0.999 m_M$, with which the massive daughter particles are produced with a velocity kick $v_{\text{kick}} \simeq 1 - m_{D1}/m_M = 0.001$. We expect time evolutions of perturbations depend on whether the scale of perturbations is inside or outside the horizon, as well as whether the DDM has decayed or not. Therefore in what follows we separately investigate cases with $a_d < a_{hc}$ and $a_d > a_{hc}$.

³ We note that undersampling of the phase space of the daughter particles at $a \lesssim 10^{-4} a_D$ little affects cosmological observables as the daughter particles are energetically irrelevant and hardly affect the metric perturbations at this epoch.

3.1.1 Perturbations crossing the horizon after the decay time

Let us first consider perturbations which cross the horizon after the decay of DDM, i.e. $a_d < a_{\text{hc}}$. Here we adopt $\Gamma^{-1} = 6$ Myr and consider evolutions of perturbations at $k = 8 \times 10^{-4} h\text{Mpc}^{-1}$. This setup corresponds to $a_d \simeq 5 \times 10^{-3}$ and $a_{\text{hc}} \simeq 0.1$. In figure 1, we plot time evolutions of perturbation quantities of the mother and daughter particles, including density perturbations δ_i , pressure ones π_{Li} , energy fluxes θ_i and shear stresses σ_i . Note that regarding perturbed quantities of the mother particles, only the density perturbation δ_M is nonzero due to the vanishing momentum distribution of the mother particles and our choice of gauge.

Before the decay of DDM $a < a_d$, the density perturbations of the daughter particles δ_{D1} and δ_{D2} grow in proportion to δ_M . It is because monopole moments $\Delta f_{Dm(0)}$ are sourced by the density perturbation of the mother particles δ_M and the metric perturbation h_L , which also grow during the matter-domination epoch. In particular, sufficiently prior to the decay time in the matter-dominated Universe, δ_{D1} and δ_{D2} are related to δ_M as

$$\delta_{D1} = \delta_M, \quad (3.1)$$

$$\delta_{D2} = \frac{23}{21}\delta_M, \quad (3.2)$$

on superhorizon scales, which can be derived analytically as in Appendix A. Our numerical result is consistent with analytic one as seen in the upper left panel of figure 1.

Since the massive daughter particles are non-relativistic, their pressure perturbations are suppressed as $\delta p_{D1} \simeq \mathcal{O}(v_{\text{kick}}^2)\delta\rho_{D1}$, while that of the massless daughter one is large as $\delta p_{D2} = \delta\rho_{D2}/3$. As can be seen in eq. (2.36) dipole moments $\Delta f_{Dm(1)}$ are sourced only by monopole and quadrupole moments via free-streaming. At superhorizon scales $k < \pi\tau^{-1}$, therefore dipole moments $\Delta f_{Dm(1)}$ and hence the energy fluxes θ_{Dm} are little generated. On the other hand, as quadrupole moments $\Delta f_{Dm(2)}$ are directly generated by metric perturbations (see eq. (2.36)), σ_{Dm} can be large. In addition, for the same reason as the pressure perturbation δp_{D1} , velocity-weighted quantities of the massive daughter particles, including θ_{D1} and σ_{D1} , are further suppressed.

After the decay of DDM but still before the horizon crossing $a_d < a < a_{\text{hc}}$, daughter particles are no longer sourced by the mother particles and the last term of eq. (2.35) becomes negligible. In this epoch, the Boltzmann equations for the daughter particles become the same as that for collisionless free-streaming particles, e.g. massive neutrinos (see ref. [23]). For non-relativistic particles, the evolution equation of Δf_{D1} should be effectively reduced to that of CDM. Hence the density fluctuation of the massive daughter particles evolves in the same way as the mother ones. Due to redshifting of physical momenta, higher-order velocity-weighted quantities such as π_{LD1} , θ_{D1} and σ_{D1} decrease afterward. For the massless daughter particles, the evolution equation of Δf_{D2} becomes the same as that of massless neutrinos.

After the horizon crossing $a > a_{\text{hc}}$, the daughter particles start free-streaming. The free-streaming length of the massless daughter particles equals to the size of horizon and perturbation quantities decay oscillating. For massive daughter particles, the

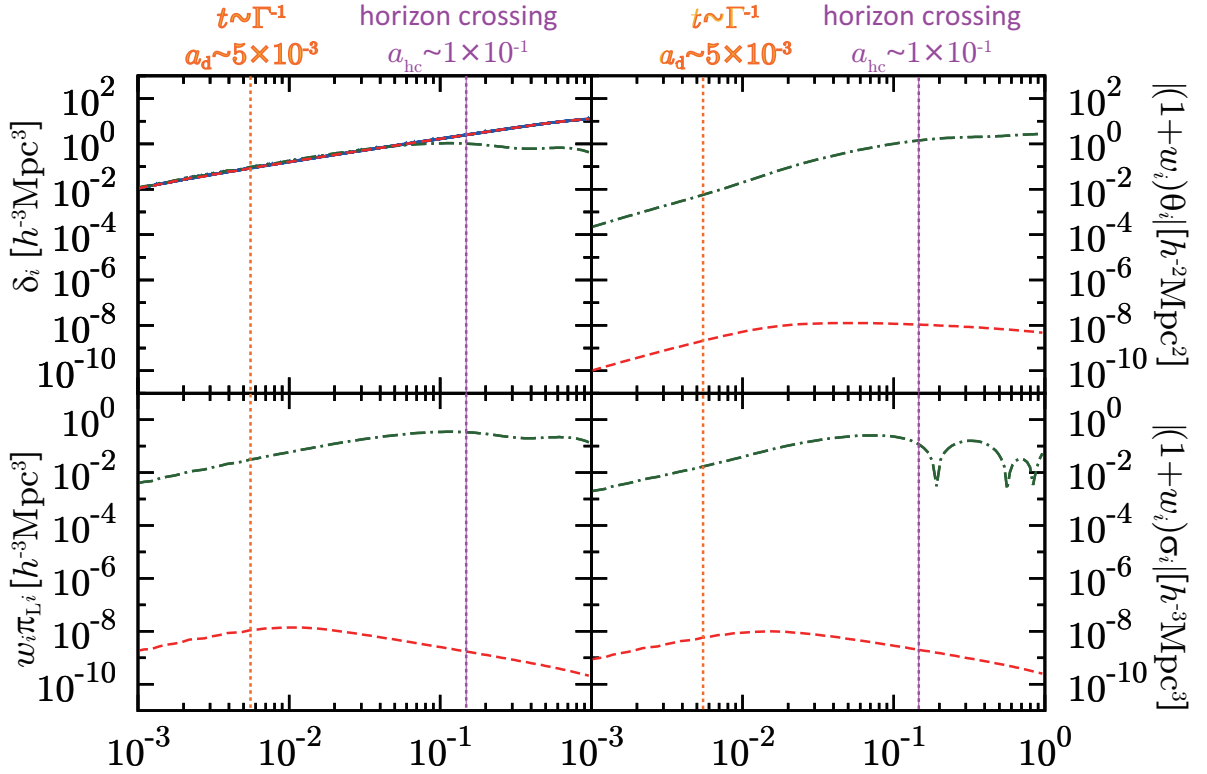


Figure 1. Time evolutions of perturbations in the case of non-relativistic decay. Here we show perturbations whose scale $k = 8 \times 10^{-4} h\text{Mpc}^{-1}$ crosses the horizon after the decay time $\Gamma^{-1} = 6$ Myr. Shown are the density perturbations (top left), energy fluxes (top right), pressure perturbations (bottom left) and anisotropic stresses (bottom right) of the mother (blue solid line), massive daughter (red dashed line) and massless daughter (green dot-dashed line) particles. In the upper left panel, the line of the density perturbation of the massive daughter overlaps that of the mother particle. Two dotted vertical lines indicate the horizon crossing and the decay time. $w_i = \bar{p}_i/\bar{\rho}_i$ is the equation of state of the i -th component. According to our gauge choice, the dipole and quadrupole moment of the mother particle are zero. Thus the energy flux and anisotropic stress of mother particle are zero. In addition, because of our assumption that the momentum of mother particle is negligible compared with its mass, the pressure perturbation of mother particle becomes zero. Therefore these quantities of mother particle, such as θ_M , π_M and σ_M , are zero and not shown in upper right and bottom panels.

density perturbation δ_{D1} continues to grow inside the horizon in the same way as CDM, while the velocity-weighted quantities continue to decay due to redshifting of momentum.

3.1.2 Perturbations crossing the horizon before the decay time

Now we move to a case where DDM decays inside the horizon. We set the decay time to $\Gamma^{-1} = 0.1$ Gyr, which corresponds to $a_d \simeq 3 \times 10^{-2}$, and investigate perturbations on a scale $k = 8 \times 10^{-3} h\text{Mpc}^{-1}$, which crosses the horizon at $a_{hc} \simeq 2 \times 10^{-3}$. Time

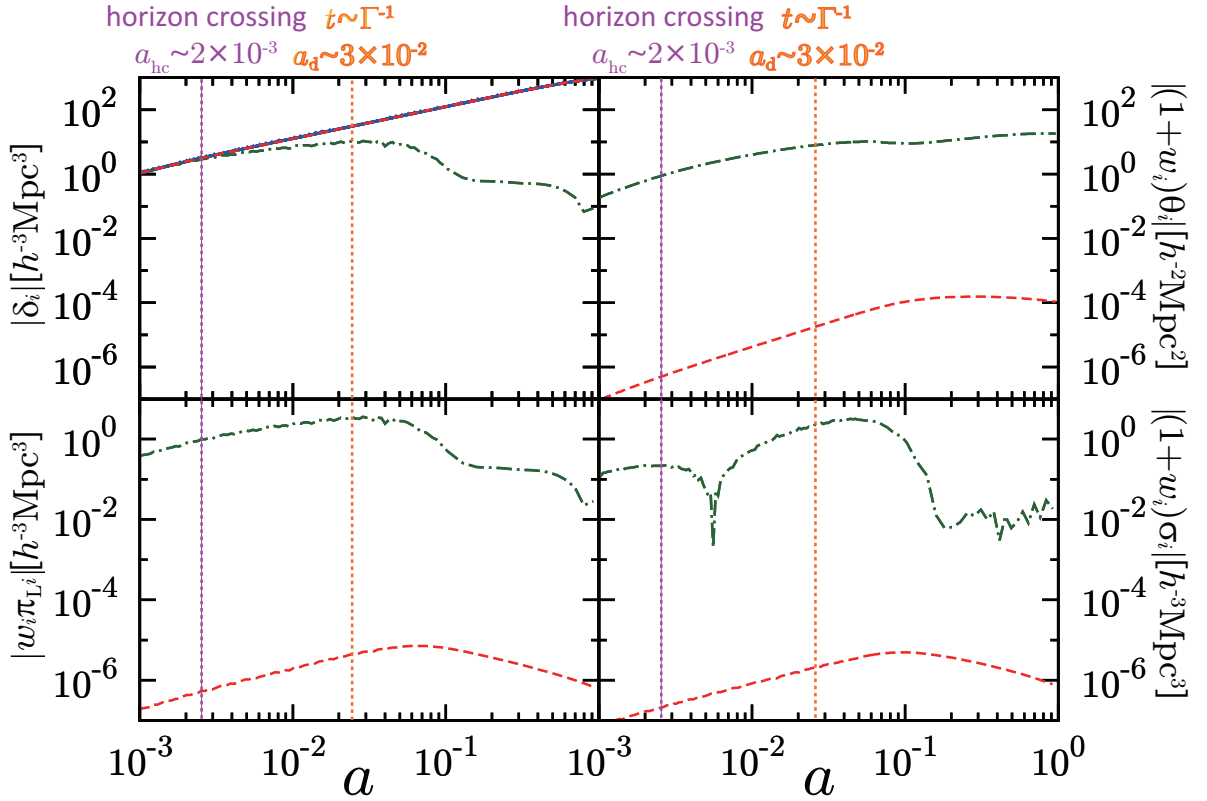


Figure 2. Same as in figure 1 but for $\Gamma^{-1} = 0.1$ Gyr and $k = 8 \times 10^{-3} h\text{Mpc}^{-1}$. In the upper left panel, the line of the density perturbation of the massive daughter overlaps that of the mother particle as same as figure 1.

evolutions of perturbed quantities related to the mother and daughter particles are plotted in figure 2.

By comparing figure 2 with figure 1, we can say that at superhorizon scales when $a < a_{\text{hc}}$ and in this case inevitably before the decay, behaviors of perturbed quantities of the mother and daughter particles are qualitatively the same as in the previous case where the horizon crossing occurs after the decay. In particular, the analytical solutions of eqs. (3.1) and (3.2) again hold at superhorizon scales, which can be qualitatively confirmed in the upper left panel of figure 2.

On the other hand, evolutions of perturbations inside the horizon drastically differ from those in the previous case. After the horizon crossing but still before the decay $a_{\text{hc}} < a < a_{\text{d}}$, the massless daughter particles start to free-stream. However, as we can see in figure 2, the perturbation quantities, such as $\delta_{\text{D}2}$, $\theta_{\text{D}2}$ and $\sigma_{\text{D}2}$ do not start to oscillate nor decay, contrary to those in figure 1. This is because the monopole moment of the massless daughter particles $\Delta f_{\text{D}2(0)}$ is continuously sourced by the density perturbation of the mother particles, and then the dipole and higher multipole moments are also continuously sourced by $\Delta f_{\text{D}2(0)}$. Therefore perturbation quantities of free-streaming relativistic particles keep on growing even inside the horizon. Moreover, as for the massive daughter particles, higher-order velocity-weighted quantities including

π_{LD1} , θ_{LD1} and σ_{LD1} also grow. This is because the massive daughter particles with the nonzero velocity $v_{\text{kick}} = 0.001$ keep on being produced, and these particles with relatively large momenta free-stream to make higher-order velocity-weighted quantities grow continuously in addition to the density perturbation $\delta\rho_{\text{D1}}$.

Finally at $a > a_{\text{d}}$, when there are few mother particles to decay, the source terms in the Boltzmann eqs. (2.35)-(2.38) for the daughter particles become ineffective and these particles behave as collisionless free-streaming particles. Perturbation quantities of the massless daughter particles start to oscillate and decay due to free-streaming. Comparing figure 2 with figure 1, we can see perturbation quantities of the massless daughter particles decay more quickly and effects of free-streaming are more prominent than the previous case. This is because most of the daughter particles are produced when $a \simeq a_{\text{d}}$ and these particles immediately free-stream over distances larger than the perturbation scale. On the other hand, since the massive particles are non-relativistic, effects of free-streaming is not significant and higher-order velocity-weighted quantities decrease mostly due to redshifting of momentum.

3.2 A case of relativistic decay

In this subsection, we consider a case with $m_{\text{D1}} \ll m_{\text{M}}$, which we refer to as relativistic decay. Here we adopt $m_{\text{D1}} = 0.1m_{\text{M}}$, which gives a velocity kick of the massive daughter particles $v_{\text{kick}} \simeq 1 - 2(m_{\text{D1}}/m_{\text{M}})^2 = 0.98$. In the same way as section 3.1, we in the following explore time evolutions of perturbations in cases with $a_{\text{d}} < a_{\text{hc}}$ and $a_{\text{hc}} < a_{\text{d}}$ separately.

3.2.1 Perturbations crossing the horizon after the decay time

Let us see time evolutions of perturbations whose scale crosses the horizon after the decay time. We adopt a decay time $\Gamma^{-1} = 6$ Myr and the scale of perturbations is fixed to $k = 8 \times 10^{-4} h\text{Mpc}^{-1}$. These parameters lead to $a_{\text{d}} = 5 \times 10^{-3}$ and $a_{\text{hc}} = 5 \times 10^{-2}$. Figure 3 shows time evolutions of perturbation quantities of the mother and daughter particles.

First of all, we expect cosmological effects of the two daughter particles are identical as long as both of them are sufficiently relativistic. Noting that momenta of particles scale as a^{-1} , the time when most of the massive daughter particles become non-relativistic can be estimated as $a_{\text{nr}} = (v_{\text{kick}}/\sqrt{1 - v_{\text{kick}}^2})a_{\text{d}}$, which is roughly 2.5×10^{-2} with the parameter values we adopted here. Therefore when $a < a_{\text{nr}}$, perturbation quantities of the two daughter particles are almost the same, which can be confirmed in figure 3.

One big difference from the case of non-relativistic decay is that the density perturbations δ_i grow more rapidly after the decay at superhorizon scales as can be seen in the upper left panel of figure 3. The reason can be understood as follows. Since the decay products are relativistic, the Universe is effectively dominated by radiation after the decay. Therefore, as in the radiation-dominated epoch, density perturbations grow as a^2 at superhorizon scales instead of a in the matter-dominated epoch (see eqs. (A.9) and (A.20)). As seen in the ΛCDM model with low Ω_{m} (we refer to, e.g., ref. [28]), this leads to an enhancement in the matter power spectrum at scales which crosses

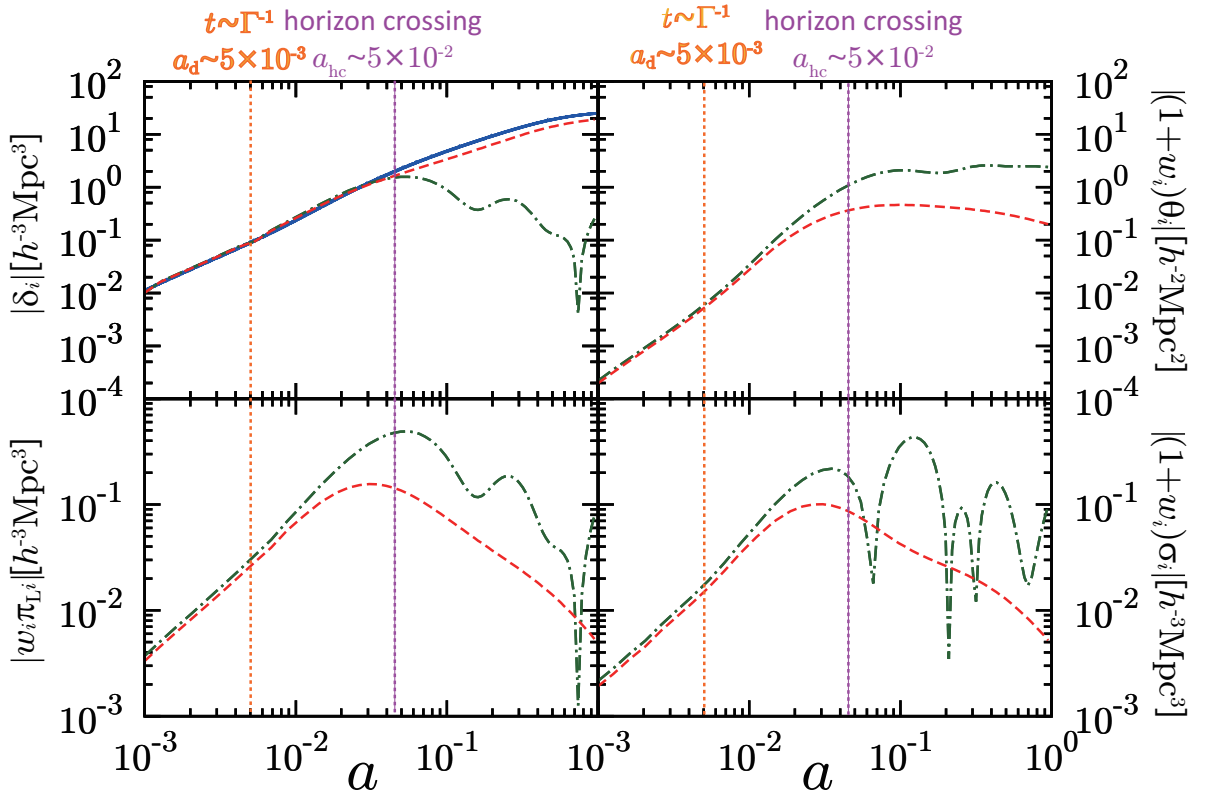


Figure 3. Same as in figure 1 but for $m_{D1}/m_M = 0.1$.

the horizon after the matter-radiation equality. This issue will be discussed further in section 4.2.

After horizon crossing, even when $a > a_{nr}$, due to the non-vanishing velocity and free streaming of daughter particles, at first growth of δ_{D1} is slower compared with the case of non relativistic decay (see also the upper left panel of figure 1). This leads that the density perturbation of the mother particles δ_M also grows less, for the gravitational potential sourced by δ_{D1} decays inside the horizon. After the massive daughter particles become fully non-relativistic, their density perturbation starts to grow as CDM does. Other perturbation quantities with higher velocity-weights such as π_{LD1} , θ_{D1} and σ_{D1} start decreasing almost monotonically without violent oscillations, which is also seen in cases of non-relativistic decay (see the upper right and bottom panel of figure 1). The massless particles keep on free-streaming and their perturbations except for velocity divergence continuously decay.

3.2.2 Perturbations crossing the horizon before the decay time

Figure 4 shows time evolutions of perturbations for a case where the decay occurs inside the horizon. Here we adopt $\Gamma^{-1} = 0.1$ Gyr and show perturbations at a scale $k = 8 \times 10^{-3} h\text{Mpc}^{-1}$. These parameters correspond to $a_d \simeq 3 \times 10^{-2}$ and $a_{hc} = 2 \times 10^{-3}$. In this case, most of the massive daughter particles become non-relativistic at around $a_{nr} = (v_{kick}/\sqrt{1-v_{kick}^2})a_d \simeq 0.15$.

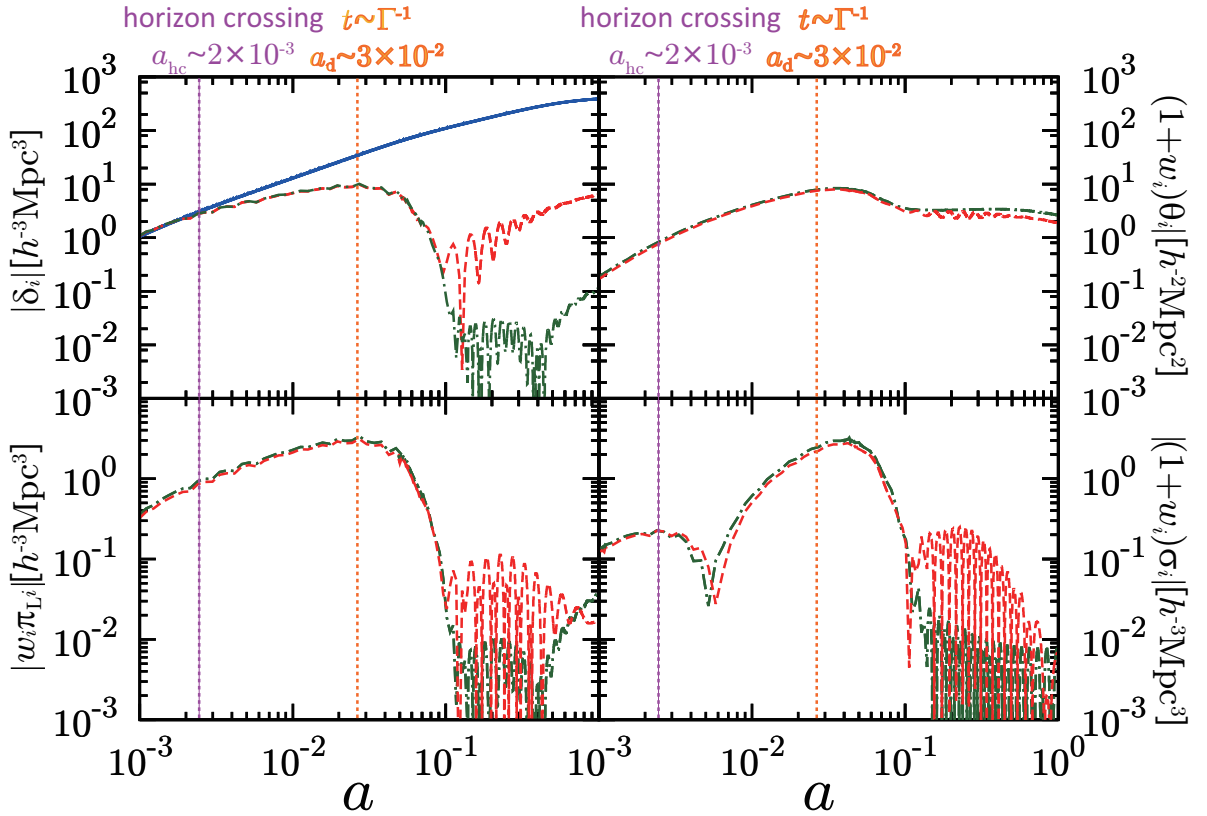


Figure 4. Same as in figure 2, but for $m_{D1}/m_M = 0.1$. Some jaggy features on plots are caused by the numerical error on the calculation.

At $a < a_{nr}$, as expected, the perturbation evolutions of the two daughter particles are again almost the same, which can be seen in figure 4. As is discussed in the case of non-relativistic decay in section 3.1, in this case perturbation quantities continuously grow inside the horizon until the mother particles completely decay, and then effects of free-streaming become significant. This can be confirmed in figure 4.

As the massive daughter particles become non-relativistic at $a > a_{nr}$ their density perturbation δ_{D1} starts to grow and other velocity-weighted perturbations π_{LD1} etc. start to decrease with less oscillation than before. However, the decay of δ_{D1} is so significant, the density perturbation of total matter becomes much smaller than the density perturbations of the mother particles δ_M . This decay of the density perturbation leads to a significant suppression in the matter power at small scales as will be shown in section 4.2. On the other hand, the massless daughter particles continuously free-stream.

4 Signatures in cosmological observables

4.1 Effects on C_l

In this subsection, we consider the CMB power spectrum C_l in the DDM models with $\Gamma^{-1} > t_*$. In figure 5, we plot the CMB temperature power spectrum C_l^{TT} with various decay times $0.01 < \Gamma^{-1} [\text{Gyr}] < 100$ and mass ratios $0.3 < m_{\text{D1}}/m_{\text{M}} < 0.9$. From the figure, we can see effects of DDM on C_l^{TT} are twofold. First one is the shift of the positions of the acoustic peaks caused by a change in the background expansion. The other is the integrated Sachs-Wolfe effect induced by the decay of the gravitational potential.

Let us first investigate the effects on positions of the acoustic peaks. When Γ^{-1} is shorter than the age of the Universe at present $t_{\text{age}} \simeq 14 \text{ Gyr}$ [25] and DDM decays into the relativistic daughter particles, energy density in the Universe and hence the expansion rate stay below those in the ΛCDM model. This makes angular diameter distances larger and hence the angular size of the sound horizon smaller than in the case of the ΛCDM model. Therefore positions of the acoustic peaks shift toward higher l .

Second, let us move to the effects that arise at large angular scales larger than the sound horizon at the recombination epoch. At these scales, CMB temperature anisotropy can be given as [23, 29]

$$\frac{\delta T}{T}(\mathbf{n}) = \frac{1}{3}\psi(\mathbf{x}_*, \tau_*) + \int_{\tau_*}^{\tau_{\text{now}}} d\tau \left(\dot{\phi}(\mathbf{x}, \tau) + \dot{\psi}(\mathbf{x}, \tau) \right) \quad , \quad (4.1)$$

where $\mathbf{x} = (\tau_{\text{now}} - \tau)\mathbf{n}$, $\phi(\mathbf{x}, \tau)$ and $\psi(\mathbf{x}, \tau)$ are the curvature perturbation and the gravitational potential, respectively. They are given in terms of the metric perturbations in the synchronous gauge as $\phi = \eta_{\text{T}} - (\mathcal{H}/2k^2)(\dot{h}_{\text{L}} + 6\dot{\eta}_{\text{T}})$ and $\psi = 1/2k^2 \left((\ddot{h}_{\text{L}} + 6\ddot{\eta}_{\text{T}}) + \mathcal{H}(\dot{h}_{\text{L}} + 6\dot{\eta}_{\text{T}}) \right)$ [23]. The second term in eq. (4.1) shows that a time derivative of the curvature perturbation $\dot{\phi}$ and that of gravitational potential $\dot{\psi}$ generate additional CMB temperature fluctuations on large scales, which is called the integrated Sachs-Wolfe (ISW) effect. As we have shown in section 3, in the DDM models density perturbations of daughter particles and hence the gravitational potentials can decay at $t > \Gamma^{-1}$, due to free-streaming of the daughter particles. This leads to a large ISW effect. From figure 5, one can find that the effect is enhanced as $m_{\text{D1}}/m_{\text{M}}$ decreases, which can be easily understood as we have seen that the suppression of density perturbation δ_{D1} is more significant in case of the relativistic decay than in the non-relativistic decay in section 3. On the other hand, one can recognize that the largest l where C_l^{TT} is enhanced decreases as Γ^{-1} increases. This is because the ISW effect is only effective at scales larger than the free-streaming scale of the daughter particles within which the gravitational potential decays. At smaller scales, photons travel through a number of peaks and troughs of the gravitational potential and the net effect of the potential decay becomes negligible.

Finally, let us describe signatures in the CMB polarization spectrum C_l^{EE} and its cross-correlation with the temperature anisotropy C_l^{TE} . In figures 6 and 7, we plot

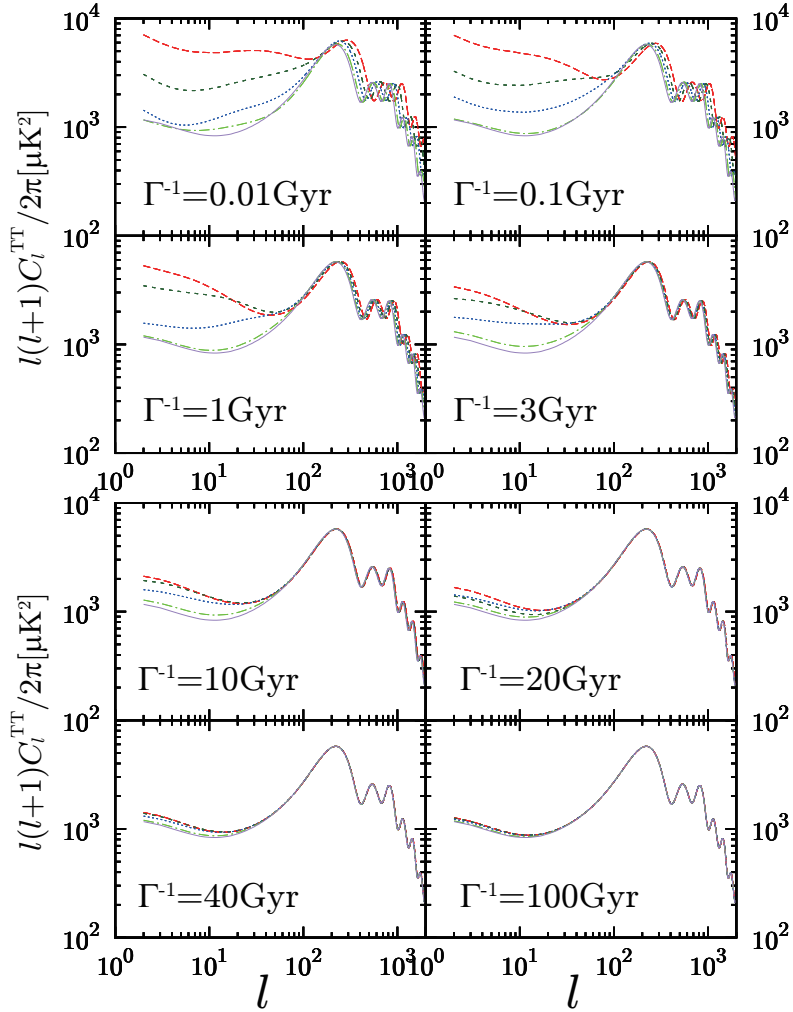


Figure 5. Effects of DDM on CMB power spectrum of temperature fluctuation C_l^{TT} . Line color distinguishes the mass ratio $m_{\text{D1}}/m_{\text{M}}$. Red (long-dashed), dark-green (short-dashed), blue (dotted), green (dot-dashed) lines represent $m_{\text{D1}}/m_{\text{M}} = 0.3, 0.5, 0.7,$ and $0.9,$ respectively. Purple (solid) lines correspond to C_l^{TT} in the ΛCDM model. Each panel shows C_l^{TT} with a distinct decay time Γ^{-1} , which varies from 0.01 (top left) to 100 Gyr (bottom right) as indicated in each panel.

C_l^{EE} and C_l^{TE} , respectively, with the same parameter sets as in figure 5. First, we can see that the DDM models affect C_l^{EE} and C_l^{TE} through the change in the background expansion. Therefore in the same way as C_l^{TT} , acoustic peaks and troughs in C_l^{EE} and C_l^{TE} shift toward higher l in the DDM models. Second, in figures 6 and 7 we can also see that there arises an additional E-mode polarization for $\Gamma^{-1} < 3$ Gyr at $l \sim 10$. Because the decay of dark matter causes an additional ISW effect, temperature fluctuations are created at a superhorizon scale. Just after horizon crossing, the quadrupole moment of temperature fluctuations is created due to the free-streaming of CMB photons. In addition, free-streaming motion of daughter particles create a nonzero shear

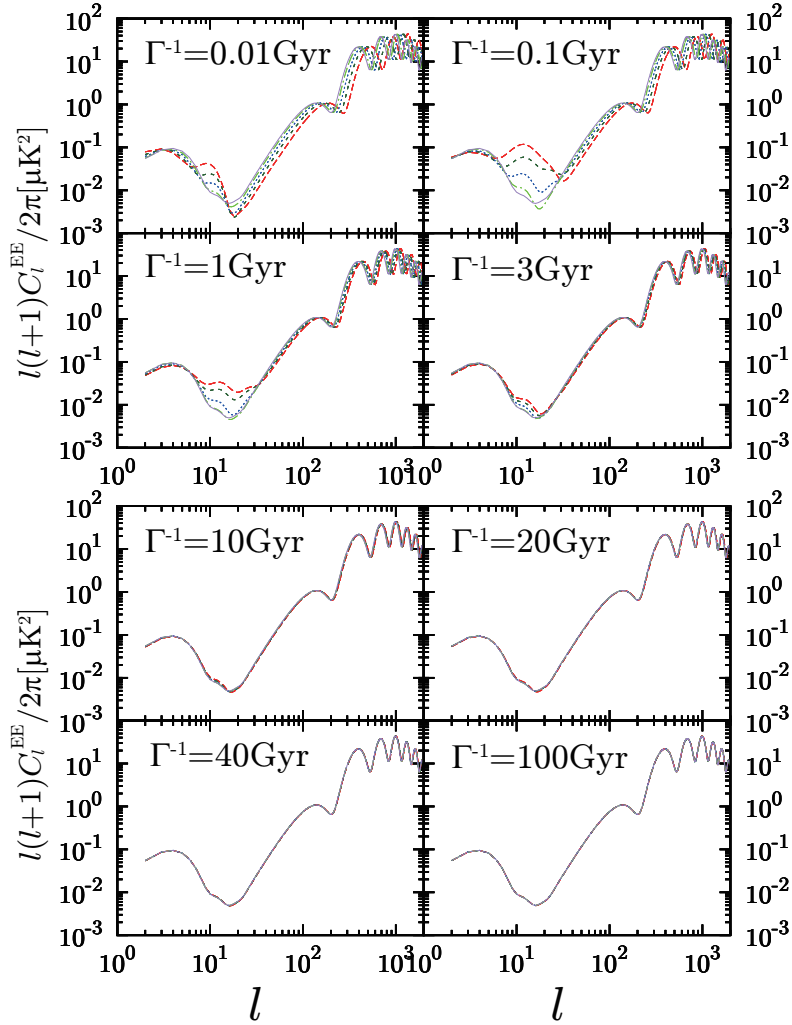


Figure 6. Same as figure 5 , but for C_l^{EE} .

stress and hence induce the anisotropic part of the metric perturbations, which also generates the quadrupole moment of the temperature fluctuations. After the cosmological reionization, the E-mode polarization is created from the quadrupole moment of the temperature anisotropy by the Thomson scattering. When one considers the epoch well after cosmological recombination, the number density of free electrons reaches a maximum in the epoch of the cosmological reionization. Thus, the decay of DDM generates the additional E-mode polarization significantly if the decay occurs around the reionization epoch at $l \sim 10$, which corresponds to the view angle of the horizon size at the cosmological reionization.

When DDM decays much earlier or much later than the cosmological reionization epoch, the additional quadrupole moment of the CMB temperature anisotropy at the reionization epoch is small and the signatures of DDM in C_l^{EE} or C_l^{TE} become insignificant.

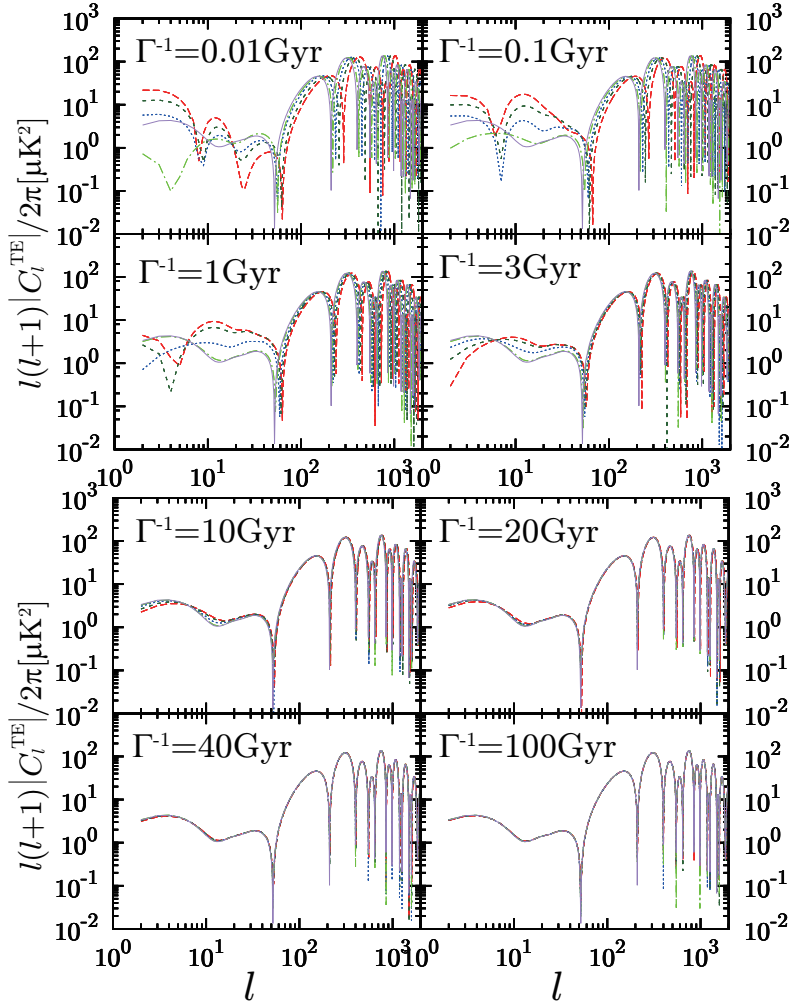


Figure 7. Same as figure 5 , but for C_l^{TE} .

4.2 Effects on $P(k)$

Let us consider effects of the decay of DDM on the matter power spectrum $P(k)$. As we will see, effects from the decay are more prominent in $P(k)$ than in C_l , so that we may obtain stronger constraints from observations of $P(k)$ than from those of C_l .

In figure 8, we plot the matter power spectra $P(k)$ in the DDM models with various lifetimes Γ^{-1} and mass ratios $m_{\text{D1}}/m_{\text{M}}$. In the same figure we also plot $P(k)$ for the Λ CDM model as a reference. From the figure, one can find that there arise two large differences from the Λ CDM model in $P(k)$. The first one is the suppression at smaller scales. This suppression is caused by the free-streaming of the daughter particles, as we have discussed in section 3. The other one is the enhancement at large scales. This enhancement is caused by the growth of density perturbations at superhorizon scales after the decay of DDM, which we have also discussed in section 3.2.1. These changes are significant if the decay time is smaller than the age of the Universe and the mass difference between the mother and daughter particles are large.

On the other hand, if the decay time is larger than the age of the Universe, a significant fraction of the mother particles, whose density perturbation grows as that of CDM, still survive until today and the deviations in $P(k)$ from the Λ CDM model become less prominent.

To clarify the cause of the changes in $P(k)$, in figure 9 we plot $P(k)$ for various decay time $\Gamma^{-1} = 0.01, 0.1, 0.3$ and $1 \text{ Gyr} \ll t_{\text{age}}$ with a fixed mass ratio $m_{\text{D1}}/m_{\text{M}} = 0.7$. As a reference, we also plot $P(k)$ of the flat Λ CDM model in which the CDM density parameter is changed from the fiducial value Ω_{c} to $m_{\text{D1}}/m_{\text{M}} \times \Omega_{\text{c}}$ so that the energy density of dark matter in the present Universe should be the same as in the DDM models. As we attribute the suppression at small scales to the free-streaming of the daughter particles, we in addition plot the free-streaming scales of the massive daughter particles λ_{FSS} , which can be approximately given as

$$\lambda_{\text{FSS}} = \int_{\tau_{\text{d}}}^{\tau_0} d\tau v(\tau) \sim \frac{v_{\text{kick}}}{H_0 \sqrt{\Omega_{\text{M}}}} \int_{a_{\text{d}}}^1 da \frac{1}{a^{-1/2} \sqrt{q^2 + m^2 a^2}} \sim \frac{3v_{\text{kick}} \Gamma^{-1}}{a_{\text{d}}}, \quad (4.2)$$

where we assumed that the background expansion does not deviate significantly from that in the reference Λ CDM model, which is a good approximation in the case of $m_{\text{D1}}/m_{\text{M}} = 0.7$. As is expected, we can see that the scales of the suppressions roughly agree with the free-streaming scales of the massive daughter particles. We can also see that the matter power spectra in the DDM models asymptotically become the same as that in the reference Λ CDM model. This shows that the enhancement in $P(k)$ at large scales seen in figure 8 is explained by the reduction in the energy density of dark matter, which effectively changes the matter-radiation equality and growth of the density perturbations at superhorizon scales.

5 Discussion

In order to illuminate the difference of the power spectrum between DDM and Λ CDM, we plot $P(k)$ in the DDM models normalized by that of the Λ CDM model, $P(k)/P_{\Lambda\text{CDM}}(k)$ with several parameter sets $(\Gamma^{-1}, m_{\text{D1}}/m_{\text{M}})$ in figure 10. In the figure we find asymptotic plateaus on small scales, especially in the plots for small $m_{\text{D1}}/m_{\text{M}}$ ratios. In the small-scale limit $k \rightarrow \infty$, we find the ratio r to be

$$r = \frac{P(k)}{P_{\Lambda\text{CDM}}(k)} \sim \left(\exp\left(-\frac{t_{\text{age}}}{\Gamma^{-1}}\right) \right)^2. \quad (5.1)$$

Thus, r is responsible for the energy density of the surviving mother particles. Therefore precise measurements of the matter power spectrum enable us to distinguish DDM from the warm dark matter (WDM) models, because these models predict that the power spectrum monotonically decreases to zero as k increases on smaller scales⁴, although that of DDM approaches asymptotically to a constant r on these scales.

⁴For example, Bode et al. mentions that the matter power spectrum in a WDM model decreases in proportion to k^{-10} on smaller scales [30].

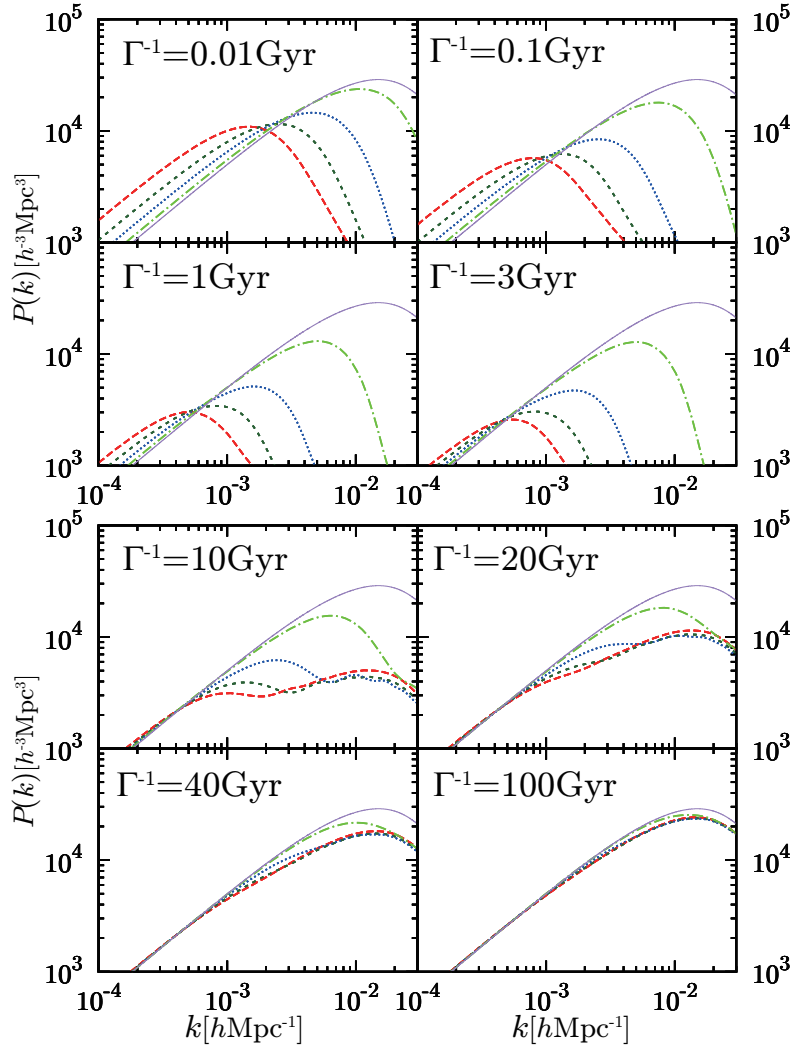


Figure 8. $P(k)$ for the DDM model with various parameters (Γ^{-1} , $m_{\text{D1}}/m_{\text{M}}$). Red (long-dashed), dark-green (short-dashed), blue (dotted), green (dot-dashed) lines represent cases with $m_{\text{D1}}/m_{\text{M}} = 0.3, 0.5, 0.7, 0.9$, respectively. Purple (solid) line corresponds to the Λ CDM model.

In order to set a constraint on the parameters of the DDM models, Γ^{-1} and $m_{\text{D1}}/m_{\text{M}}$, we quantify the effect of DDM on $\sigma_{(R)}$, which is the fluctuation amplitude at scale R in units of $h^{-1}\text{Mpc}$. Given $P(k)$, $\sigma_{(R)}$ can be obtained as

$$\sigma_{(R)}^2 = 4\pi \int_0^\infty dk k^2 W^2(kR) P(k) , \quad (5.2)$$

where $W(kR)$ is defined as

$$W(kR) \equiv \frac{3}{(kR)^3} (\sin(kR) - kR \cos(kR)) , \quad (5.3)$$

by employing the top hat window function.

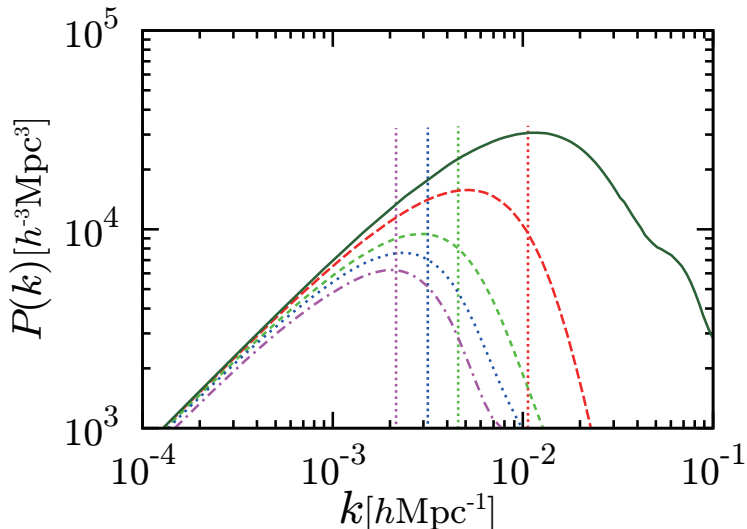


Figure 9. Matter power spectrum at present for several parameter sets with $\Gamma^{-1} \ll t_{\text{age}}$. On this graph we fixed $m_{\text{D1}}/m_{\text{M}}$ to 0.7. Red (long-dashed), green (short-dashed), blue (dotted), purple (dot-dashed) lines represent $P(k)$ in the case that the lifetime of DDM $\Gamma^{-1} = 0.01, 0.1, 0.3,$ and 1 Gyr, respectively. Dotted lines correspond to the free streaming scales $k_{\text{FSS}} = \pi/\lambda_{\text{FSS}}$ calculated from eq. (4.2) in these parameter sets, which correspond to $2.1, 3.1, 4.7,$ and $10 [\times 10^{-3} h\text{Mpc}^{-1}]$, respectively. Dark-green line shows $P(k)$ in a case of the ΛCDM model whose dark matter density parameter Ω_{c} is replaced with $m_{\text{D1}}/m_{\text{M}} \times \Omega_{\text{c}}$. Note that these parameter sets have been already excluded in our previous work [26].

We calculate the fluctuation amplitude at $8 h^{-1}\text{Mpc}$, σ_8 , in the DDM model and compare it to observations [31–34]. Recently, σ_8 is reported as [33]

$$\sigma_8 = 0.80 \pm 0.02. \quad (5.4)$$

We rule out the parameter region where $\sigma_8^{(\text{th})}$ deviates from eq. (5.4) by more than 2σ confidence level as shown in figure 11. In the same figure, we also depict constraints from Peter [17] and Wang et al.[22], which we referred to in introduction.

To understand the constraint in figure 11, it is convenient to consider cases $\Gamma^{-1} > t_{\text{age}}$ and $\Gamma^{-1} < t_{\text{age}}$ separately. First, in the case of $\Gamma^{-1} > t_{\text{age}}$, not all of the mother particles have decayed by now. As Γ^{-1} increases, more mother particles survive in the present Universe and the deviation from the ΛCDM model becomes less. Therefore, depending on the fractional mass difference $m_{\text{D1}}/m_{\text{M}}$, small Γ^{-1} is excluded. In particular, when the decay is to some extent relativistic, that is, $m_{\text{D1}}/m_{\text{M}} \lesssim 0.9$, $\Gamma^{-1} \gtrsim 200$ Gyr is allowed. We think the reason why the lower bound on Γ^{-1} hardly depends on $m_{\text{D1}}/m_{\text{M}}$ is that the daughter particles have a velocity kick which is close to the speed of light. This result is consistent with previous works [7, 13, 17, 26]. On the other hand, when the decay is highly non-relativistic, $m_{\text{D1}}/m_{\text{M}} > 0.998$, the lifetime of DDM is not constrained, since the evolution of the decay products is indistinguishable from that of CDM. Second, in the case of $\Gamma^{-1} < t_{\text{age}}$, all the mother particles decay into the daughter particles. In this case how $P(k)$ is suppressed can be under-

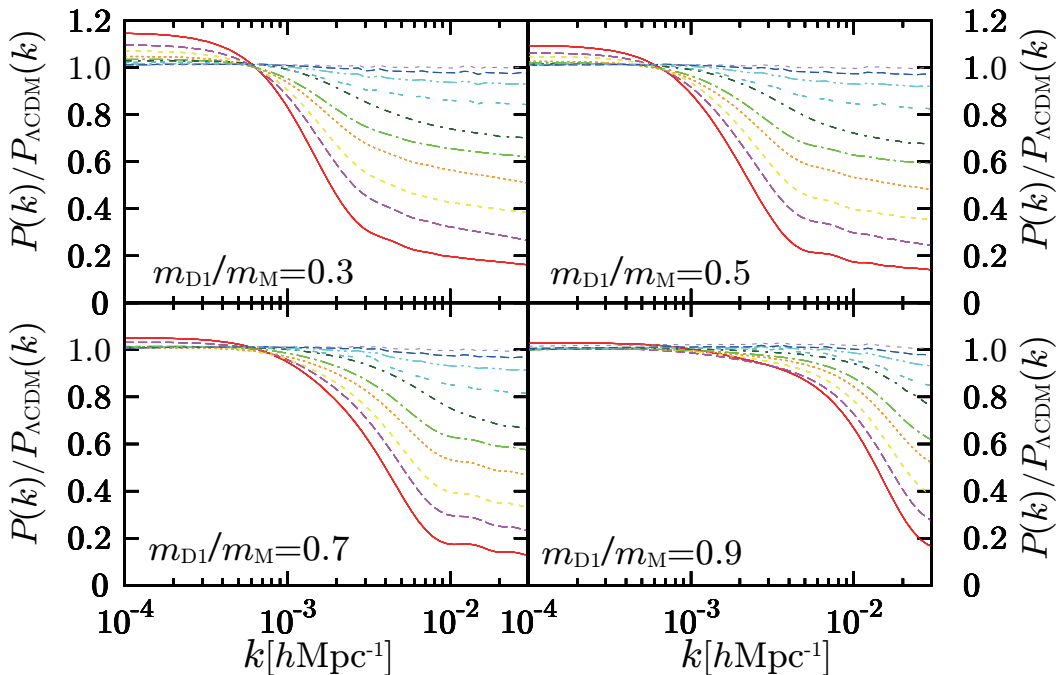


Figure 10. The ratio of $P(k)$ to the matter power spectrum in the Λ CDM model $P_{\Lambda\text{CDM}}$. Lines from bottom to top represent numerically-obtained values in the case of $\Gamma^{-1} = 10, 15, 20, 30, 40, 50, 100, 200, 400,$ and 800 Gyr, respectively. Different panels show $P(k)$ with different mass ratios $m_{\text{D1}}/m_{\text{M}}$ which are 0.3 (top left), 0.5 (top right), 0.7 (bottom left) and 0.9 (bottom right).

stood in terms of the free-streaming length λ_{FSS} , as is discussed in the literature, e.g. ref. [26]. Therefore a parameter region with a large mass difference $1 - m_{\text{D1}}/m_{\text{M}}$ is excluded in figure 11. As we have mentioned in section 4.2, given a fixed $m_{\text{D1}}/m_{\text{M}}$, λ_{FSS} decreases as the mother particles decay earlier and the suppression becomes less significant. Therefore the constraint on the mass difference becomes weaker as the lifetime Γ^{-1} becomes smaller.

Let us remark on constraints from CMB data. As we have shown, DDM models affect the CMB temperature power spectrum effectively in two ways: shifting the angular scale of the acoustic oscillation and enhancing the ISW effect. The constraint from the former effect was derived in Aoyama et al.[26], and we have found that it is less strong than one we here derived from σ_8 . On the other hand, we also expect that the latter effect would not be so powerful as σ_8 due to the cosmic variance.

We should note that the constraint on Γ^{-1} and $m_{\text{D1}}/m_{\text{M}}$ we derived here is over-estimated, as we fixed other cosmological parameters which may degenerate with these two parameters. We will pursue this issue in future works.

5.1 Implication on the anomaly in estimated σ_8 from Planck

Planck collaboration reports that the estimated σ_8 from their cluster number count through the SZ effect is $\sigma_8 = 0.78 \pm 0.01$, which is smaller than that from the anisotropy

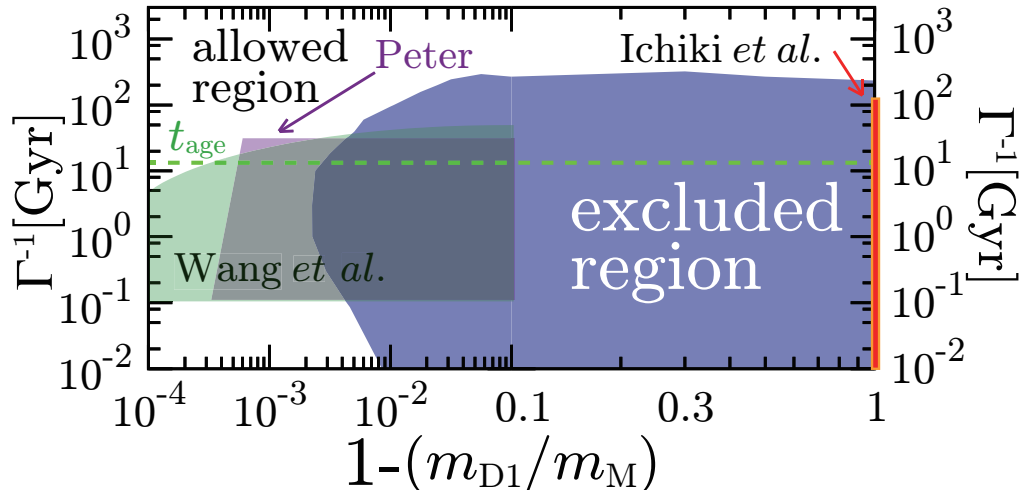


Figure 11. Constraint on the lifetime of DDM and the mass ratio of the massive daughter particle to the mother particle. The blue shaded region represents the excluded parameter region at 2σ confidence level from a constraint of σ_8 [33]. The green (dashed) line presents the age of the Universe at present $t_{\text{age}} = 13.8$ Gyr. The purple, green and red shaded regions are the parameter regions which Peter [17], Wang et al. [22] and Ichiki et al. [7] have excluded, respectively.

of the CMB $\sigma_8 = 0.834 \pm 0.027$ by more than 2σ confidence level [35]. Because the number of clusters reflects the matter perturbation in the late-time Universe, this discrepancy in the estimated σ_8 may indicate some mechanisms which suppress the matter perturbation at small scales after cosmological recombination. The DDM model may reconcile the discrepancy, because the decay of DDM with the lifetime slightly larger than the age of the universe can suppress the matter power at present keeping the CMB power spectrum almost unchanged. In figure 12, we plot a parameter region which can explain the estimated σ_8 obtained from the cluster number count in this DDM model at the 1σ confidence level with the cosmological parameters obtained by Planck [25], i.e. $(\Omega_b, \Omega_c, h_0, \tau_{\text{opt}}, n_s, A_s) = (0.04900, 0.2671, 0.6711, 0.0925, 0.9675, 2.215 \times 10^{-9})$.

We see in figure 12 that $\Gamma^{-1} \simeq 200$ Gyr is favored if $1 - m_{\text{D1}}/m_{\text{M}} \gtrsim 10^{-1}$, in which case DDM decays into two relativistic particles. On the other hand, $\Gamma^{-1} < t_{\text{age}}$ is favored if $m_{\text{D1}}/m_{\text{M}} \sim 1 - 10^{-2.5}$, in which case the massive daughter particles are non-relativistic when they are produced. However this parameter region has been already excluded by Peter [17] and Wang et al. [22]. Peter is due to observations of the halo mass-concentration and galaxy-cluster mass function. Wang et al. is due to small scale structures observed by Lyman- α Forest, which should not be destroyed by decaying of dark matter.

While the DDM model with $\Gamma \gtrsim 200$ Gyr and $1 - (m_{\text{D1}}/m_{\text{M}}) \gtrsim 0.1$ may be able to solve the discrepancy in σ_8 estimated from the CMB power spectrum and the SZ cluster counts of Planck, one may wonder such models can be constrained by the CMB lens power spectrum $C_l^{\phi\phi}$. In figure 13, we compare $C_l^{\phi\phi}$ in the DDM model

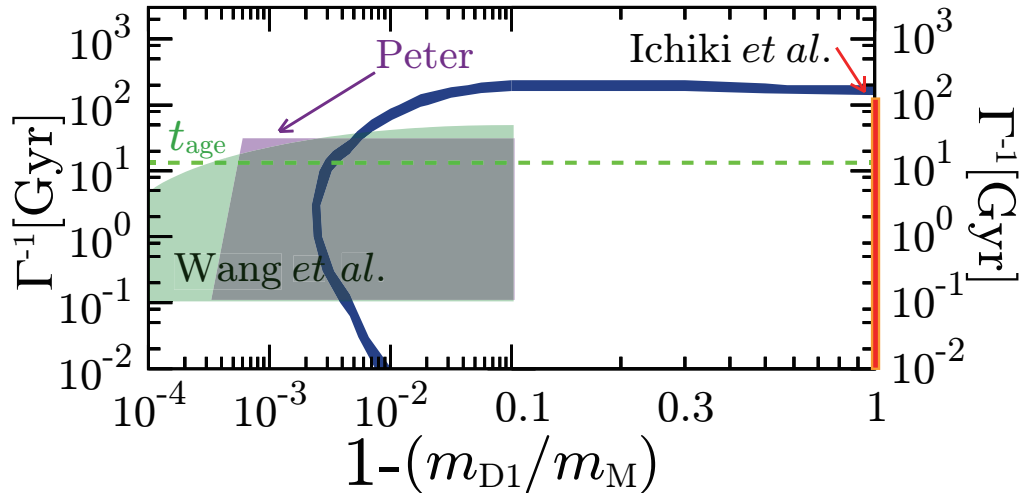


Figure 12. The parameter region which can explain the tension in the estimated σ_8 from the SZ effect cluster number count and from C_l^{TT} at 1σ confidence level. The parameter regions excluded in previous studies are also shown in the figure. The purple, green and red regions are the same as in figure 11.

with the observational result which was reported by the Planck paper [36]. The figure shows that the dark matter decaying suppresses $C_l^{\phi\phi}$ compared with that in the ΛCDM model. However, it seems that the current data is not constraining enough for such the parameter region to be excluded. We defer a more quantitative analysis to future work.

6 Conclusion

In this paper, we considered cosmological consequences of the DDM model where the cold mother particles decay into massive and massless particles. In particular, we focused on evolutions of cosmological perturbations in the model and their signatures in the CMB power spectrum C_l and the matter power spectrum $P(k)$. While similar kinds of models had been studied by various authors, we for the first time explored cases with an arbitrary mass ratio between the daughter and mother particles $m_{\text{D1}}/m_{\text{M}}$. For this purpose, we solved the phase space distributions of the decay products. To summarize, the main effect of the decay of DDM is that the free-streaming of the daughter particles suppresses structure formation at scales smaller than the free-streaming length.

As for CMB, the DDM model mainly affects the temperature anisotropy at large angular scales through the ISW effect. A constraint on Γ^{-1} and $m_{\text{D1}}/m_{\text{M}}$ from the peak shift of C_l^{TT} has been set on Aoyama et al.[26]. Their constraint from it is $\Gamma^{-1} > 30$ Gyr at $m_{\text{D1}}/m_{\text{M}} \ll 1$. However, since measurements of C_l at large angular sales are fundamentally limited by the cosmic variance, CMB may not be a promising probe of the DDM model. On the other hand, the matter power spectrum $P(k)$ is affected by dark matter decaying significantly even when $\Gamma^{-1} \gg t_{\text{age}}$. Indeed, by

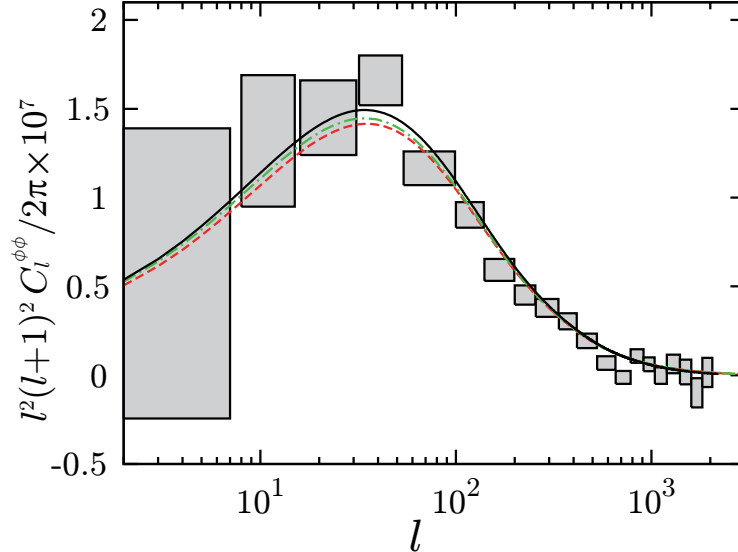


Figure 13. The effect of DDM on the CMB lensing potential power spectrum $C_l^{\phi\phi}$. The shaded boxes are the data from the Planck experiment [36]. Red (dashed) and green (dot-dashed) lines represent cases with $m_{D1}/m_M = 0.3$ and 0.9 , respectively. In both cases, the lifetime of DDM is set to be $\Gamma^{-1} = 200$ Gyr. For comparison, the black (solid) line represents the case in the Λ CDM model.

using the observational data of σ_8 [33], we succeeded in excluding parameter region in the 2D plane of the fractional mass difference between the daughter and mother particles and the decay time. If the decay product is relativistic, the decay time Γ^{-1} should be longer than 200 Gyr, and if the decay time is shorter than the age of the Universe, the fractional mass difference $1 - m_{D1}/m_M$ should be smaller than $10^{-2.5}$. The tension between estimated σ_8 from the SZ effect and the CMB angular power spectrum in the recent Planck data may be explained by the DDM model if Γ^{-1} is around 200 Gyr and the decay products are relativistic.

Acknowledgments

We thank Masahiro Takada for discussions and valuable suggestions. T.S. is supported by the Academy of Finland grant 1263714. This work is supported in part by scientific research expense for Research Fellow of the Japan Society for the Promotion of Science from JSPS (24009838)(S.A.) and (23005622) (T.S.) and Grant-in-Aid for Scientific Research Nos. 22012004 (K.I.), 25287057 (N.S.) of the Ministry of Education, Sports, Science and Technology (MEXT) of Japan, and also supported by Grant-in-Aid for the Global Center of Excellence program at Nagoya University "Quest for Fundamental Principles in the Universe: from Particles to the Solar System and the Cosmos" from the MEXT of Japan. This research has also been supported in part by World Premier International Research Center Initiative, MEXT, Japan.

A Initial condition for the perturbed distribution functions of the daughter particles

In this appendix, we first derive the solution of the perturbed phase space distribution $\Delta f_{Dm(l)}$ at $\tau = \tau_q$. This gives the initial condition needed in solving the perturbation evolution numerically. As a side product, we then also derive the analytic solution of the density perturbations of the daughter particles at superhorizon scales well before the decay time.

For later convenience, let us rewrite the solution eq. (2.34) for the background distribution function $\bar{f}_D(q, \tau)$ as

$$\bar{f}_D(q, \tau) \equiv F_D(q) \Theta(ap_{D\max} - q), \quad (\text{A.1})$$

where

$$F_D(q) = \frac{a_q \Gamma \bar{N}_M(\tau_q)}{4\pi q^3 \mathcal{H}_q}, \quad (\text{A.2})$$

which is a smooth function of q and does not depend on τ . When the decay of the mother particles can be neglected, their comoving number density can be approximated as $\bar{N}_M(\tau) = \bar{N}_{M\emptyset}$. Thus at $t \ll \Gamma^{-1}$ we can approximate eq. (A.2) as

$$F_D(q) \approx \frac{a_q \Gamma \bar{N}_{M\emptyset}}{4\pi q^3 \mathcal{H}_q}. \quad (\text{A.3})$$

Adopting eq. (A.2), eq. (2.35) can be rewritten as

$$\frac{\partial \Delta f_{Dm(0)}}{\partial \tau} = -\frac{qk}{\epsilon_{Dm}} \Delta f_{Dm(1)} + \frac{\dot{h}_L}{6} q \frac{dF_D}{dq} \Theta(\tau - \tau_q) + \left[-\frac{\dot{h}_L}{6\mathcal{H}} + \delta_M \right] F_D \delta(\tau - \tau_q) \quad (\text{A.4})$$

By integrating eq.(A.4) in an infinitesimal interval around $\tau = \tau_q$, we obtain

$$\Delta f_{Dm(0)}(q, \tau_q) = \left[-\frac{\dot{h}_L(\tau_q)}{6\mathcal{H}_q} + \delta_M(\tau_q) \right] F_D(q). \quad (\text{A.5})$$

In the same way, eq. (2.37) can be rewritten as

$$\begin{aligned} \frac{\partial \Delta f_{Dm(2)}}{\partial \tau} &= \frac{qk}{(2l+1)\epsilon_{Dm}} \left[l \Delta f_{Dm(1)} - (l+1) \Delta f_{Dm(3)} \right] \\ &\quad - \left[\frac{\dot{h}_L}{15} + \frac{2\dot{\eta}_T}{5} \right] q \frac{dF_D}{dq} \Theta(\tau - \tau_q) + \frac{1}{\mathcal{H}} \left[\frac{\dot{h}_L}{15} + \frac{2\dot{\eta}_T}{5} \right] F_D \delta(\tau - \tau_q) \end{aligned} \quad (\text{A.6})$$

which leads to

$$\Delta f_{Dm(2)}(q, \tau_q) = \frac{1}{\mathcal{H}_q} \left[\frac{\dot{h}_L(\tau_q)}{15} + \frac{2\dot{\eta}_T(\tau_q)}{5} \right] F_D(q). \quad (\text{A.7})$$

On the other hand, for $l \neq 0, 2$, as the right hand side of Eqs (2.35) and (2.38) are smooth around $\tau = \tau_q$, we obtain

$$\Delta f_{Dm(l)}(q, \tau_q) = 0 \quad (\text{for } l \neq 0, 2). \quad (\text{A.8})$$

A.1 Radiation-dominated era

Now let us consider the superhorizon solution well before the decay time. In radiation-dominated era, δ_M at superhorizon scales, \mathcal{H} and a can be related to τ as follows (see e.g. ref. [23]).

$$\delta_M \propto \tau^2, \quad (\text{A.9})$$

$$\mathcal{H} = \tau^{-1}, \quad (\text{A.10})$$

$$a \propto \tau. \quad (\text{A.11})$$

By substituting eqs. (A.9) and (A.10) into eq. (2.29) one can derive a relation

$$\dot{h}_L = -2\dot{\delta}_M = -4\mathcal{H}\delta_M. \quad (\text{A.12})$$

Substituting eqs. (A.12) into eq. (A.5), we obtain

$$\Delta f_{Dm(0)}(q, \tau_q) = \frac{5}{3}F_D(q)\delta_M(\tau_q). \quad (\text{A.13})$$

Furthermore, by substituting eq. (A.10) into eq. (A.3) and $\tau_q \propto q$, one can find

$$F_D(q) \propto q^{-1}, \quad (\text{A.14})$$

$$q \frac{dF_D}{dq} = -F_D. \quad (\text{A.15})$$

Then in the limit of $k\tau \rightarrow 0$, eq. (A.4) in conjunction with eq. (A.13) gives

$$\begin{aligned} \Delta f_{Dm(0)}(q, \tau) &= \left(\left[\frac{1}{6} h_L q \frac{\partial F_D}{\partial q} \right]_{\tau_q}^{\tau} + \frac{5}{3} F_D(q) \delta_M(\tau_q) \right) \Theta(ap_{D\max} - q) \\ &= F_D(q) \left[\frac{1}{3} \delta_M(\tau) + \frac{4}{3} \delta_M(\tau_q) \right] \Theta(ap_{D\max} - q). \end{aligned} \quad (\text{A.16})$$

Using eqs. (A.9) and (A.11), we then obtain

$$\Delta f_{Dm(0)}(q, \tau) = \frac{1}{3} F_D(q) \delta_M(\tau) \left[1 + 4 \left(\frac{a_q}{a} \right)^2 \right] \Theta(ap_{D\max} - q). \quad (\text{A.17})$$

Note that this result does not depend on the particle index m . By substituting eq. (A.17) into eq. (2.39), we can compute the density perturbation δ_{Dm} . When the decay products are relativistic $p_{D\max} \gg m_{Dm}$, we obtain

$$\delta_{Dm}(\tau) = \frac{17}{15} \delta_M(\tau). \quad (\text{A.18})$$

Finally, when the decay products are non-relativistic $p_{D\max} \ll m_{Dm}$, we obtain

$$\delta_{Dm}(\tau) = \delta_M(\tau). \quad (\text{A.19})$$

A.2 Matter-dominated era

In the matter-dominated era well before the decay time, δ_M at superhorizon scale, \mathcal{H} and a can be related to τ as [23]

$$\delta_M(\tau) \propto \tau^2, \quad (\text{A.20})$$

$$\mathcal{H} = 2\tau^{-1}, \quad (\text{A.21})$$

$$a \propto \tau^2. \quad (\text{A.22})$$

Then one can find eq. (A.12) should be replaced with

$$\dot{h}_L = -2\mathcal{H}\delta_M, \quad (\text{A.23})$$

with which eq. (A.13) should be replaced with

$$\Delta f_{Dm(0)}(q, \tau_q) = \frac{4}{3}F_D(q)\delta_M(\tau_q). \quad (\text{A.24})$$

By substituting eqs. (A.21) and (A.22) into eq. (A.3), we obtain

$$F_D \propto q^{-3/2}, \quad (\text{A.25})$$

$$q \frac{dF_D}{dq} = -\frac{3}{2}F_D. \quad (\text{A.26})$$

Then from eqs. (A.4) and (A.24), in the limit $k\tau \rightarrow 0$ we obtain

$$\Delta f_{Dm(0)}(q, \tau) = \frac{1}{2}F_D(q)\delta_M(\tau) \left[1 + \frac{5a_q}{3a} \right] \Theta(ap_{D\max} - q). \quad (\text{A.27})$$

In the same way as in radiation-dominated epoch, by substituting eq. (A.27) into eq. (2.39), we can compute the density perturbation δ_{Dm} . When they are relativistic, we obtain

$$\delta_{Dm} = \frac{23}{21}\delta_M, \quad (\text{A.28})$$

while when the decay products are non-relativistic, we obtain

$$\delta_{Dm} = \delta_M. \quad (\text{A.29})$$

References

- [1] Planck Collaboration *et al.*, *Planck 2013 results. I. Overview of products and scientific results*, ArXiv e-prints (Mar., 2013) [[1303.5062](#)].
- [2] G. Gentile *et al.*, *The cored distribution of dark matter in spiral galaxies*, MNRAS **351** (July, 2004) 903–922 [[astro-ph/0403154](#)].
- [3] J. van Eymeren *et al.*, *Non-circular motions and the cusp-core discrepancy in dwarf galaxies*, A&A **505** (Oct., 2009) 1–20 [[0906.4654](#)].

- [4] B. Moore *et al.*, *Dark Matter Substructure within Galactic Halos*, ApJ **524** (Oct., 1999) L19–L22 [[arXiv:astro-ph/9907411](#)].
- [5] C. W. Purcell, A. R. Zentner, *Bailing out the Milky Way: variation in the properties of massive dwarfs among galaxy-sized systems*, J. Cosmology Astropart. Phys. **12** (Dec., 2012) 7 [[1208.4602](#)].
- [6] R. Cen, *Decaying Cold Dark Matter Model and Small-Scale Power*, ApJ **546** (Jan., 2001) L77–L80 [[arXiv:astro-ph/0005206](#)].
- [7] K. Ichiki, M. Oguri, K. Takahashi, *Constraints from the Wilkinson Microwave Anisotropy Probe on Decaying Cold Dark Matter*, Physical Review Letters **93** (Aug., 2004) 071302–+ [[arXiv:astro-ph/0403164](#)].
- [8] M. Oguri *et al.*, *Decaying Cold Dark Matter and the Evolution of the Cluster Abundance*, ApJ **597** (Nov., 2003) 645–649 [[arXiv:astro-ph/0306020](#)].
- [9] A. H. G. Peter, C. E. Moody, M. Kamionkowski, *Dark-matter decays and self-gravitating halos*, Phys. Rev. D **81** (May, 2010) 103501–+ [[1003.0419](#)].
- [10] M. Kaplinghat, *Dark matter from early decays*, Phys. Rev. D **72** (Sept., 2005) 063510 [[arXiv:astro-ph/0507300](#)].
- [11] M. Kaplinghat *et al.*, *Improved treatment of cosmic microwave background fluctuations induced by a late-decaying massive neutrino*, Phys. Rev. D **60** (Dec., 1999) 123508–+ [[arXiv:astro-ph/9907388](#)].
- [12] M. Kawasaki, G. Steigman, H.-S. Kang, *Cosmological evolution of an early-decaying particle*, Nuclear Physics B **403** (Aug., 1993) 671–706.
- [13] S. DeLope Amigo *et al.*, *Cosmological constraints on decaying dark matter*, J. Cosmology Astropart. Phys. **6** (June, 2009) 5–+ [[0812.4016](#)].
- [14] L. A. Anchordoqui *et al.*, *Hunting long-lived gluinos at the Pierre Auger Observatory*, Phys. Rev. D **77** (Jan., 2008) 023009–+ [[0710.0525](#)].
- [15] G. Bertone, D. Hooper, J. Silk, *Particle dark matter: evidence, candidates and constraints*, Phys. Rep. **405** (Jan., 2005) 279–390 [[arXiv:hep-ph/0404175](#)].
- [16] M. Kawasaki, K. Kohri, T. Moroi, *Hadronic decay of late-decaying particles and big-bang nucleosynthesis*, Physics Letters B **625** (Oct., 2005) 7–12 [[arXiv:astro-ph/0402490](#)].
- [17] A. H. G. Peter, *Mapping the allowed parameter space for decaying dark matter models*, Phys. Rev. D **81** (Apr., 2010) 083511–+ [[1001.3870](#)].
- [18] N. F. Bell, A. J. Galea, R. R. Volkas, *Model for late dark matter decay*, Phys. Rev. D **83** (Mar., 2011) 063504–+ [[1012.0067](#)].
- [19] R. Huo, *Constraining decaying dark matter*, Physics Letters B **701** (July, 2011) 530–534 [[1104.4094](#)].
- [20] O. Eggers Bjaelde, S. Das, A. Moss, *Origin of ΔN_{eff} as a result of an interaction between dark radiation and dark matter*, J. Cosmology Astropart. Phys. **10** (Oct., 2012) 17 [[1205.0553](#)].
- [21] M.-Y. Wang, A. R. Zentner, *Effects of unstable dark matter on large-scale structure and constraints from future surveys*, Phys. Rev. D **85** (Feb., 2012) 043514 [[1201.2426](#)].

- [22] M.-Y. Wang *et al.*, *Lyman- α forest constraints on decaying dark matter*, Phys. Rev. D **88** (Dec., 2013) 123515 [[1309.7354](#)].
- [23] C.-P. Ma, E. Bertschinger, *Cosmological Perturbation Theory in the Synchronous and Conformal Newtonian Gauges*, ApJ **455** (Dec., 1995) 7 [[arXiv:astro-ph/9506072](#)].
- [24] E. Komatsu *et al.*, *Seven-year Wilkinson Microwave Anisotropy Probe (WMAP) Observations: Cosmological Interpretation*, ApJS **192** (Feb., 2011) 18 [[1001.4538](#)].
- [25] Planck Collaboration *et al.*, *Planck 2013 results. XVI. Cosmological parameters*, ArXiv e-prints (Mar., 2013) [[1303.5076](#)].
- [26] S. Aoyama *et al.*, *Formulation and constraints on decaying dark matter with finite mass daughter particles*, J. Cosmology Astropart. Phys. **9** (Sept., 2011) 25 [[1106.1984](#)].
- [27] A. Lewis, A. Challinor, A. Lasenby, *Efficient Computation of Cosmic Microwave Background Anisotropies in Closed Friedmann-Robertson-Walker Models*, ApJ **538** (Aug., 2000) 473–476 [[arXiv:astro-ph/9911177](#)].
- [28] S. Dodelson, Modern cosmology. Academic Press, 2003.
- [29] U. Seljak, M. Zaldarriaga, *A Line-of-Sight Integration Approach to Cosmic Microwave Background Anisotropies*, ApJ **469** (Oct., 1996) 437 [[arXiv:astro-ph/9603033](#)].
- [30] P. Bode, J. P. Ostriker, N. Turok, *Halo Formation in Warm Dark Matter Models*, ApJ **556** (July, 2001) 93–107 [[arXiv:astro-ph/0010389](#)].
- [31] H. Lin *et al.*, *The SDSS Co-add: Cosmic Shear Measurement*, ApJ **761** (Dec., 2012) 15 [[1111.6622](#)].
- [32] D. Parkinson *et al.*, *The WiggleZ Dark Energy Survey: Final data release and cosmological results*, Phys. Rev. D **86** (Nov., 2012) 103518 [[1210.2130](#)].
- [33] A. G. Sánchez *et al.*, *The clustering of galaxies in the SDSS-III Baryon Oscillation Spectroscopic Survey: cosmological implications of the large-scale two-point correlation function*, MNRAS **425** (Sept., 2012) 415–437 [[1203.6616](#)].
- [34] A. van Engelen *et al.*, *A Measurement of Gravitational Lensing of the Microwave Background Using South Pole Telescope Data*, ApJ **756** (Sept., 2012) 142 [[1202.0546](#)].
- [35] Planck Collaboration *et al.*, *Planck 2013 results. XX. Cosmology from Sunyaev-Zeldovich cluster counts*, ArXiv e-prints (Mar., 2013) [[1303.5080](#)].
- [36] Planck Collaboration *et al.*, *Planck 2013 results. XVII. Gravitational lensing by large-scale structure*, ArXiv e-prints (Mar., 2013) [[1303.5077](#)].